General Disclaimer

One or more of the Following Statements may affect this Document

- This document has been reproduced from the best copy furnished by the organizational source. It is being released in the interest of making available as much information as possible.

- This document may contain data, which exceeds the sheet parameters. It was furnished in this condition by the organizational source and is the best copy available.

- This document may contain tone-on-tone or color graphs, charts and/or pictures, which have been reproduced in black and white.

- This document is paginated as submitted by the original source.

- Portions of this document are not fully legible due to the historical nature of some of the material. However, it is the best reproduction available from the original submission.

Progress Report

on

INVESTIGATIONS AND ANALYSIS OF FLOW PHENOMENA OF SECONDARY MOTIONS IN AXIAL FLOW INDUCERS

By

R. Lakshminarayana

prepared from work done under

NASA Grant ~~NsG 537/39-009-007~~ NGL-39-009-007

Department of Aerospace Engineering
The Pennsylvania State University
University Park, Pa.

JUNE 1969

Progress Report on

INVESTIGATIONS AND ANALYSIS OF FLOW PHENOMENA OF SECONDARY MOTIONS IN AXIAL FLOW INDUCERS

by

B. Lakshminarayana

Submitted to:

National Aeronautics and

Space Administration

Washington, D. C.

Prepared under NASA Grant No. ~~NsG 537/39-009-007~~ NGL-39-009-007 by

Department of Aerospace Engineering

The Pennsylvania State University

University Park, Pa. 16802

June, 1969

PREFACE

This report contains only a brief summary of the investigations of the flow phenomena in a four bladed inducer carried out during the nine month period ending March 31, 1969.

The analytical and experimental investigation of the turbulent boundary layer characteristics on a rotating helical blade has been concluded. A final report on this investigation is under preparation and will be submitted in about 3 - 4 weeks.

TABLE OF CONTENTS

NOMENCLATURE

W	Resultant relative velocity
V	Resultant absolute velocity
r, θ, z	Radial, tangential and axial coordinates
p	Static pressure
P_o	Stagnation pressure
$U=\Omega r$	Local Blade speed
ε_w	Angle of the limiting streamline at the blade surfaces (measured with respect to tangential direction)
ε_o	Maximum deviation of the streamline from the cylindrical surface outside the blade boundary layer (in degrees)
β	Blade angle measured from the tangential direction
α	Absolute airflow angle measured from the tangential direction
Ψ_T	Stagnation head rise coefficient $(\frac{2gJ}{U_t^2})$
δ	Boundary layer thickness
δ_1	Thickness of the secondary flow reversal region
Ψ_s	Static head coefficient
$(\Psi_T)_{Loss}$	(Ψ_T) inlet - (Ψ_T) outlet
RP	Rotating probe measurements
SP	Stationary Probe measurements
c_f	Skin friction coefficient

$R = r/r_t = \frac{\text{local radius}}{\text{tip radius}}$ of the blade

Subscripts

r,θ,Z	Components along r, θ, Z directions
Abs	Referred to absolute flow or stationary coordinate system
Rel	Referred to relative flow or rotating coordinate system
t	Refers to the values at the tip
R	Stagnation head coefficient of the relative flow
P	Pressure surface
S	Suction surface

Superscript

—	Averaged over the Passage

1. BACKGROUND OF THE PRESENT INVESTIGATION

Since November 1963, the Department of Aerospace Engineering at the Pennsylvania State University has conducted investigation of flow in pump inducers under NASA sponsorship.

A pump inducer is usually an axial flow pump-runner having an extraordinarily high "solidity" (ratio of blade length to blade spacing) and a very low "flow coefficient". (ratio of axial velocity of the fluid to the peripheral velocity of the blade). While this characteristic form is dictated by the cavitation requirements, which must be met by such inducers, the flow is subjected to major effects by the viscosity and turbulence of the fluid in the long and narrow passages between the vanes. The investigations conducted by this department have been concerned with the effects of viscosity and turbulence and not with the effects of cavitation.

During the current period of investigation, this department has designed, built and tested a three foot diameter model of an inducer which was operated in air. The flow was observed by means of smoke, flags or streamers. The fluid properties are determined at various radial, circumferential and axial locations using both, stationary and rotating probes. For the latter purpose a pressure transfer device was designed, built and tested in the laboratory. Attempts are presently made to obtain the circumferential variation of radial velocities at the outlet using an x-configuration, a hot-wire probe, and a two channel hot-wire anemometer. The results from the latter experiments are not yet conclusive.

Great difficulties are involved in carrying out experimental and analytical study of boundary layer characteristics inside a high solidity and narrow passages encountered in such axial flow inducers. To overcome some of these difficulties, the boundary layer on a simpler configuration, namely a rotating helical blade of large chord to height ratio enclosed in an annulus was studied. The objective is to investigate the boundary layer characteristics on a rotating helical surface without the influence of pressure and velocity changes that exist in an axial inducer. This investigation has been concluded and a final report on this subject matter is under preparation.

The most important observations and conclusions obtained prior to this report are the following:

1. At or near design flow coefficient, no back flow was observed at the inlet of the inducer. A separated region of flow exists near the hub at the discharge side of the inducer. This can be explained qualitatively on the basis of simplified radial equilibrium equation, when applied to the actual rather than the design head distribution. However the actual region of separation is much smaller than that derived by the condition of radial equilibrium.

Recent measurements indicate that this back flow region originates on the stationary hub just after it has left the rotating hub. Furthermore, this extent of back flow was observed to grow continuously downstream.

The extent of back flow increases considerably at the inlet of tip region and outlet hub region at flow coefficients lower than the

design value.

2. The flow visualization experiments carried out near the exposed leading part of the inducer indicate that the radial motions in the main flow (not under the influence of blade skin friction) is smaller where as the radial motions near the blade surfaces are considerable.

3. The test inducer, designed approximately for uniform head distribution over its discharge area (assuming ideal flow) actually produces a non-uniform head. Near the tip the actual head of the absolute flow was found to be 2 - 3 times that at hub and mid radius. This non-uniform head distribution can be explained qualitatively by real fluid effects and is in agreement with the observations of other investigators.

The flow survey carried out at the trailing edge and farther downstream indicate that the radial distribution of the axial velocity component changes considerably between the two stations whereas the tangential velocity profile remains the same, qualitatively. The stagnation pressure at the tip is found to decrease continuously as the flow travels downstream, whereas it remains essentially constant at mid radius and hub.

4. Measurement of the relative flow inside the blade passages (obtained with use of a rotating probe and pressure transfer device) indicate that a major portion of the total flow losses along the stream path occurs near the leading edge. This is probably due to the presence of laminar flow on the blades near the leading edge and the consequent large radial flow and associated mixing effects near the tip. The flow losses at the tip were found to be very much higher than those at other radial locations.

5. A complete flow survey of the relative flow inside the blade passage at the trailing edge recently carried out revealed the presence of a loss core located slightly inward from the blade tip. The radial movement inside the blade boundary layer, when encountered by the annulus wall tends to deflect towards the mid passage and then radially inward. The mixing effects due these secondary flows are responsible for large losses observed experimentally. The measurements indicate the presence of large loss regions near the mid passage extending all the way from mid radius to the tip region of the blades.

6. The blade boundary layers are found to be quite thin near the hub and mid radius, being thicker on suction surface than the pressure surface.

The expected radial motions within the blade passages have been qualitatively conformed by flow visualization experiments and appear to be quite strong all along the blade length.

The wall shear stress estimated from the boundary layer profiles inside the blade passage appear to be higher than that of an equivalent stationary channel having the same relative flow. Overall frictional losses estimated from the measured stagnation pressures were found to be an order of magnitude higher than that of a stationary channel having the same relative flow (based on Blausius friction coefficient for pipes).

7. At the trailing edge, the relative velocities averaged circumferentially over the passage has a maximum value near the mid radius. For a third of the blade height from the tip the relative velocities are considerably

less than their design values.

The angles of the relative flow downstream of the trailing edge were found to be nearly uniform in the circumferential direction, its deviation from the design values being greatest near the tip.

8. A new frictionloss coefficient applicable to inducers operating in the range of flow coefficients ϕ = 0.065 to 0.2 is defined and derived from the inducer data available in the open literature. This empirical friction coefficient is found to increase exponentially towards the blade tip. For the Penn State inducer, the radial variation of frictional losses estimated from this newly derived empirical loss coefficient, agrees closely with the measured values.

9. A circumferentially averaged radial equilibrium equation is used to predict the relative and absolute tangential velocities. The analysis is based on suitable assumptions for the radial and mainflow velocity profiles (based on the existing three dimensional turbulent boundary layer data available) and loss coefficients discussed in item 8. The agreement between the theory and experiment is reasonably good. Hence it is evident that if the frictional effects are known either empirically or analytically, the flow properties at the exit of the inducer can be predicted quite accurately. The very purpose of the boundary layer investigation on the helical blade and a channel is to provide the most important missing link on the frictional effects which are otherwise based on empirism and hence not universally valid.

10. The axial velocities predicted, using the continuity and axial momentum equations with assumed radial velocity profiles and the derived

tangential velocity distribution (item 9), agree qualitatively with the values measured from a stationary probe. Attempts are being made to improve the theory to include the blade blockage effect.

2. EXPERIMENTAL INVESTIGATIONS

Subsequent to our earlier report (Ref. 1) the following measurements were completed.

1) Stationary probe measurements at stations 3,4,5,6, and 7 (Fig. 1)

2) Hot wire measurements at Station 3A to derive the three dimensional flow field at the exit of the inducer (Fig. 1)

3) Annulus wall and hub wall static pressures at various axial locations of the inducer.

4) Flow visualization experiments to determine the angle of the limiting streamline (ε_w) at various radial and chordwise locations of the blades. This experiment has provided some valuable data for the theoretical analysis of the flow.

5) Complete flow survey of the relative flow at Stations (2) and (4). These measurements have revealed considerable energy loss near the tip. Substantial flow departure was observed throughout this region.

The theoretical investigation of the flow is not yet conclusive, but the measurements described above has provided very valuable information for the prediction of the flow field.

The experimental investigation of the flow in a four bladed inducer has been concluded. Measurement of the flow field in three blade inducer and improvement of the flow characteristics by boundary layer

control and by other means will be undertaken shortly. The three bladed inducer is ready for experimentation.

a) Stationary Probe Measurements (station 3, 4, 5, 6, and 7 (Fig.2-5)

In an earlier progress report (Ref. 2) flow measurements at station 5 and 6 were reported. Subsequent to this it was observed that the flow properties are changing quite considerably between trailing edge of the blade and these measuring stations. In view of this, extensive measurement of flow properties were undertaken at station 3, 4, and 7 (Fig. 1), using a stationary stagnation pressure probe, piezometric holes on the hub and wall surface. The flow angles were derived from time exposure photographs of the tuft.

In Figures 2-5 are plotted radial distribution of the static pressure coefficient [(Ψ_s)], stagnation pressure coefficient [$(\Psi_T)_{Abs}$], tangential velocity (V_θ), and axial velocity (V_Z) at various axial locations of the inducer exit. Also shown plotted for the sake of comparison is the static and stagnation pressure coefficients at station 2 (Figs. 2 & 3) derived from rotating probe measurements.

The static pressure gradient near the tip decreases slightly as the flow proceeds downstream (Fig. 2). This is partly caused by tangential momentum loss and the decay of the radial velocities.

Near the hub, a substantial decrease in stagnation pressure rise coefficient and tangential velocity was observed between stations (3) and (4) (Figures 3 & 4). This is probably caused by large axial and radial velocity gradients that exists due to blade blockage effect. Whereas the tip section experiences continuous decrease in stagnation

head as the flow proceeds downstream. (Fig. 3).

The axial velocity profiles undergo marked changes as the flow proceeds downstream. At station 3 and 4 the minimum axial velocity occurs near the mid radius, whereas at station 5 and downstream the minimum velocity occurs near the hub. (Fig. 5) These measurements indicate that the backflow region originates on the stationary hub just after it has left the rotating hub. Furthermore, the extent of backflow region was observed to grow continuously as the flow proceeds downstream. Thus in an actual pumping unit, where the inducer is an integral part of the impeller, the backflow near the hub may not be present. Large axial velocities observed near the hub, at stations 3 and 4, is probably caused by blade blockage effects. Attempts are being made to predict the changes in axial velocity due to blockage effect using Stanitz theory (Ref. 3)

b) Hot Wire Measurements

Since an accurate knowledge of the nature of radial velocities inside the blade passages is essential for the development of adequate theory for predicting the flow, an attempt was made to derive these velocity profiles using a combination of x configuration probe and single sensor probe. The probes were aligned such that it senses the following resultant velocity components.

$$V_{\theta Z} = \sqrt{V_\theta^2 + V_Z^2} \qquad (1)$$

$$V_{\theta r} = \sqrt{V_\theta^2 + V_r^2} \qquad (2)$$

$$V_{rZ} = \sqrt{V_r^2 + V_Z^2} \qquad (3)$$

Since the linearizers were found to be highly unstable, the signals from the hot wire were photographed and with the use of hot wire calibration curves, the equations (1), (2), and (3) were solved on a digital computer for various radial and tangential locations. The mean values (averaged over the time) derived from the hot wire probe is plotted and compared with conventional probe measurements in Fig. 6. Since the directions of the radial velocities cannot be sensed on a hot wire, only the RMS values derived from the hot wire is shown plotted.

The previous investigations revealed that there is considerable radial inflow near the mid passage from tip to mid radius where as the radial outflow is confined to blade boundary layers. There is conclusive evidence that the radial velocities are of the same order magnitude or higher than the axial velocities over most of the radial locations. (Fig. 6)

The variation of V_θ, V_Z and V_r across the passage at three typical radial locations are plotted in Figs. 7(a), (b), and (c).

The fact that the radial velocities are large and exists all the way across the passage near the tip region is evident from these figures (Fig. 7 a-c). The tangential velocities (V_θ) measured from the hot wire probe are in conformity with the rotating probe measurements near the hub and mid radius whereas near the tip region the magnitudes are in agreement but not the gradients $(\frac{\partial V_\theta}{r\,\partial\theta})$. Near the hub region the

radial velocities are confined only to a small distance from the blade surfaces.

The above experiment has demonstrated the feasibility of the use of hot wire anemometry for the three dimensional flow measurement at the exit of the inducer. Since there is considerable effort involved in the method used for data reduction, attempts are being made to build a sophisticated data processing equipment for the measurement of the three dimensional flow.

c) Static Pressure on the Hub and Annulus Walls (Fig. 8)

Static pressure coefficients measured on the hub walls (mid passage) and annulus walls are shown plotted in Fig. 8. Negative radial pressure gradients over part of the blade length is probably due to large radial flows and flow losses near the tip. Most of the pressure rise occurs near the trailing edge and this is in conformity with the design. There is no reasonable explanation for the negative pressures observed near the leading edge except that this might have been caused by change in incidence due to error in blade setting.

d) Limiting Streamline Angle (ε_w)

As explained in Reference 1, a knowledge of the limiting streamline angles provides very useful information on the nature and magnitude of the radial flows and the direction of the wall shear stress. With a view to obtain this information for aid in the theoretical solution of the flow, an attempt was made to derive these angles by

ammonia streak technique and smoke produced by titranium tetrachloride (Ref. 1). The radial variation of these angles (ε_w) measured at various chordwise positions are plotted in Fig. 9. For all blade locations the angle of the limiting streamline decreases linearly with radius. This is contrary to what has been observed on a single helical blade (Ref. 1). The magnitudes of ε_w are also generally higher than those observed on a single helical blade. Furthermore, ε_w increases monotonically from leading to trailing edge of the blades. These results suggest that radial velocities encountered in inducer passages, where considerable velocity and pressure gradients exist in all directions, are generally higher than those observed on a single helical blade. (Ref. 1)

The maximum deviation of the streamlines from the cylindrical surface (ε_o), outside the blade boundary layer regions, obtained from a tuft grid mounted at the exit of the inducer is shown plotted in Fig. 9. It is clear that there is substantial radial inward flow from tip to midradius. Reversal of coriolis acceleration in these regions is the cause for the large velocity deficiencies observed outside the blade boundary layers near the tip region (Fig. 10).

e) Measurement of the Relative Flow Using Rotating Probes

(Station 2 & 4 - Fig. 1)

In Reference 1, rotating probe measurements at three radial locations at station 2 were reported. In order to investigate the detailed nature of the flow behavior at various radial locations, flow survey was conducted at stations 2 and 4 using a rotating probe at ten radial locations. The

results of these measurements are shown plotted in Figures 10-15.

For the sake of brevity only the measurements at station 2 are reported in detail in this report. The measurements at station 4 indicate that the flow is nearly axisymmetric at this location. The blade to blade distribution of stagnation pressure coefficient $(\Psi_T)_R$, velocity $(\frac{W}{U_t})$ and static pressure of the relative flow at various radial locations are plotted in Fig. 10a - j. At R = 0.567, 0.621, 0.691, 0.735, and 0.761, the usual flow turning effect in addition to boundary layer growth on the blade can be seen from relative velocity plots. (figs. 10c - d) The boundary layer growth on the suction surface is generally higher than those on the pressure surface. Furthermore it can be seen that the boundary layer thickness on the suction surface is of the order of 25 percent of blade passage. Whereas the velocity profiles observed at other radial locations, R = 0.815, 0.872, and 0.925 and 0.972 (Figs. 10a - c are unconventional. An analysis of the flow near the tip carried out using an assumed radial velocity profile predicts the velocities outside the blade boundary layer qualitatively.

Using the experimentally observed fact that $W_r \frac{\partial W_O}{\partial r}$ and $W_Z \frac{W_\theta}{\partial Z}$ are small compared to other terms, the tangential momentum equation in rotating coordinates can be simplified to give,

$$W_\theta \frac{\partial W_\theta}{r\partial\theta} + \frac{W_\theta W_r}{r} - 2\Omega W_r = -\frac{1}{\rho}\frac{\partial p}{r\partial\theta} \qquad (4)$$

The assumed variation of the radial inward flow is given by,

$$W_r = \epsilon_o W_\theta \operatorname{Sin}\left(\frac{r\theta - r\theta_o}{\frac{\pi r}{4} - r\theta_o}\,\frac{\pi}{2}\right) \qquad (5)$$

where ε_o = experimentally observed maximum deviation of the streamlines outside the boundary layer region (Fig. 9), $r\theta_o$ = (Blade blockage + boundary layer thickness) in the tangential direction, $\frac{\pi r}{4}$ = blade half spacing.

Using the experimentally observed pressure gradients $(\frac{\partial p}{r\partial\theta})$, equation (4) is solved analytically using the assumed radial velocity profile (equation 5). The predicted values for R = .925 are shown in Fig. 10B. Also shown in this graph is the effect of various terms in the equation (4) It is evident that the reversal of the radial velocity is the cause for the velocity deficiencies observed outside the blade boundary layer region.

It is evident from these investigations that the radial inward flow in addition to large skin friction stresses are responsible for considerable relative flow diffusion from mid radius to tip region. A kaleidoscopic view of the variation of relative velocities is given as a contour plot in Fig. 12.

The radial variation of the average flow properties of the RELATIVE FLOW such as stagnation head coefficient $((\overline{\psi_T})_R)$, velocity $(\frac{\overline{W}}{U_t})$ and static pressure coefficients $(\overline{\psi_s})$ obtained at station (2) and (4) are shown plotted and compared in Fig. 11. From hub to mid radius, the values of $(\overline{\psi_T})_R$ is nearly the same between station 1 & 2 even though there is considerable flow diffusion (since the flow is still under the influence of the passage) as evidenced by an increase in static pressure and decrease in relative velocities. Whereas near the tip region, there is substantial increase in the values of $(\overline{\psi_T})_R$ between Station 2 and 4. This is probably caused by the partial recovery of the energy associated with the secondary flow in passages.

The contours of stagnation head coefficients of the ABSOLUTE FLOW $(\psi_T)_{ABS}$ at Station 2 derived from the rotating probe measurements, under the assumption that the blade and air angles are the same at this station, are plotted in Fig. 13(a). At the other axial location (Station 4 - Fig. 13b), the values of $(\psi_T)_{ABS}$ are derived from the relative flow angle measurements carried out by H. G. McCafferty (Reference 4). It is clear from these contour plots that large stagnation pressure rise $(\psi_T)_{Abs}$ is confined to blade boundary layers from hub to mid radius whereas at other radial locations the stagnation pressure rise is very much larger than design at all passage locations. The radial variation of the average stagnation head coefficient of the ABSOLUTE FLOW at Stations 2 and 4 are shown compared in Fig. 15. A slight increase in $(\overline{\psi_T})_{Abs}$, near the tip, between station 2 and 4 is probably caused by the partial recovery of the energy associated with the secondary flow inside the blade passages. The increase in the hub region is due to flow turning that exists between Stations 2 and 4.

The loss contours derived from the measurement of the RELATIVE FLOW according to the equation (6)

$$[(\psi_T)_R]_{loss} = [(\psi_T)_R]_{inlet} - [(\psi_T)_R]_{outlet}. \qquad (6)$$

are plotted in Fig. 14. The loss core near the corner formed by the pressure surface and annulus wall may be due to scraping of the wall boundary layer by the blade tip. The loss core near the suction surface of the tip is probably caused by the leakage flow that occurs near the blade tip. It is evident that considerable flow losses occur all across the passage from mid radius to blade tip and this is caused

by severe flow mixing and the associated turbulence stress in this region.

f) Reliability of the Rotating Probe and Stationary Probe Measurements

Considerable discrepancy between the absolute and relative flow measurements (at Station 4) were reported by F. G. McCafferty (Reference 4). These measurements were repeated and reasons for the descrepancy were found to be due to erroneous angle measurements of both the relative and absolute flow. The revised comparison of the velocity triangles derived from relative and absolute flow measurements at three typical radian locations are plotted in Figure 16(a), (b), (c). The agreement is reasonably good, thus confirming the accuracy of both types of measurement.

The radial distribution of $(\overline{\psi_T})_R$ derived from rotating and stationary probe measurements at Stations 2 and 4 are shown compared in Fig. 17. Good agreement between the two types of measurement further confirms the reliability of the results obtained from rotating probe and stationary probe measurements.

THEORETICAL INVESTIGATIONS

The status of the theoretical investigation of the flow through axial flow inducers can be broadly classified into:

a) Axial Velocity prediction at the exit of the inducer (station 2) taking into account the radial flows and the blade blockage effect. The results are not yet conclusive.

b) Tangential velocity prediction at the exit of the inducer treating it as a combination of axial flow pump and shear force

pump. The results are encouraging but are in conflict with continuity considerations. A revision of this analysis is undertaken taking into account the radial inward flow.

c) Flow prediction at exit of the inducer by momentum integral method taking into account both radial inflow and outflow at any radial location of the blade.

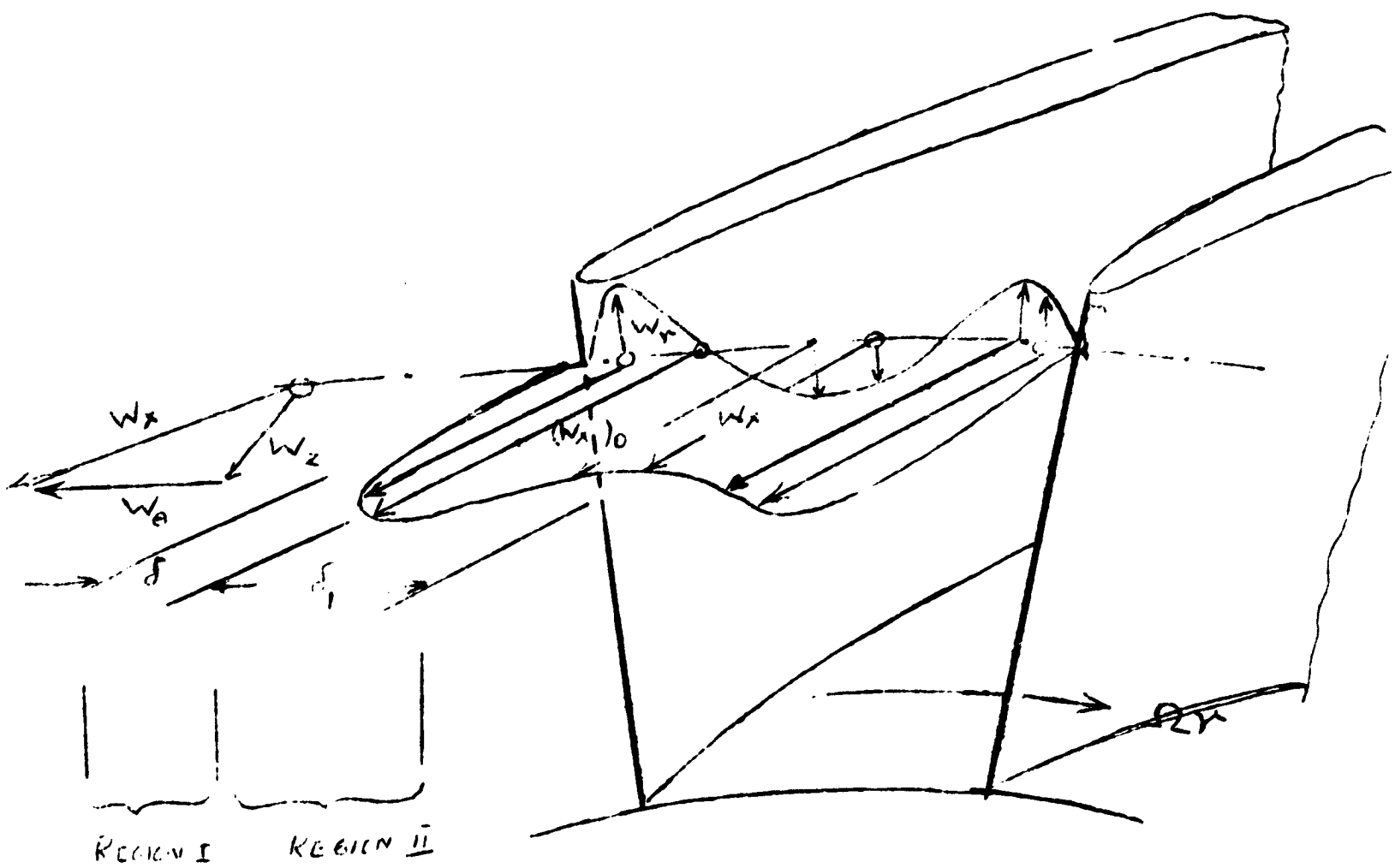

A great difficulty with the momentum integral method is that to succeed they depend very much on hindsight and ingenuity, experience and knowledgibility of particular researcher. The experimental results reported earlier provides a logical basis for the velocity profile assumptions. In a situation involving a rotating turbulent boundary layer, there are essentially no other theoretical techniques available and in these cases, the momentum integral methods become a most practical means for the flow analysis. This is the approach taken in developing a theoretical model for the inducer flow.

The figure shown above indicate the nature of the tangential and radial velocity profiles that exist from mid radius to tip section of the inducer. The momentum integral equations have the parameters $(W_\theta)_o$, δ, ε_w as the variables. If the boundary layer information is available, $(W_\theta)_o$ can be predicted and vice versa. Once the values of $(W_\theta)_o$ is known, the average tangential velocities can be computed.

If the continuity equation is substituted in the tangential momentum equation (in rotating coordinate system), the following equation results.*

$$W_r \frac{\partial W_\theta}{\partial r} - W_\theta \frac{\partial W_r}{\partial r} + W_z \frac{\partial W_\theta}{\partial Z} - W_\theta \frac{\partial W_z}{\partial Z} - 2\Omega W_r = \frac{1}{\rho}\frac{\partial \tau_w}{\partial Z} - \frac{1}{\rho}\frac{\partial p}{r\partial\theta} \quad (7)$$

$$\text{1} \qquad \text{2} \qquad \text{3} \qquad \text{4} \qquad \text{5} \qquad \text{6} \qquad \text{7}$$

If smooth flow guidance is assumed, that is the streamlines are parallel to the channel walls but not necessarily lying in a cylindrical plane then terms (3) and (4) in equation 7 are equal and thus,

$$W_r \frac{\partial W_\theta}{\partial r} - W_\theta \frac{\partial W_r}{\partial r} - 2\Omega W_r = \frac{1}{\rho}\frac{\partial \tau_w}{\partial Z} - \frac{1}{\rho}\frac{\partial p}{r\partial\theta} \quad (8)$$

* Only the dominant friction terms are retained in the equation.

using the following assumptions:

(a) $W_\theta = (W_\theta)_o (\eta)^{1/7}$, where $\eta = \frac{r\theta}{\delta}$

(b) $W_r = \epsilon_w W_\theta (1-\eta)^2$

} inside the boundary layer (Region I)

(c) $W_\theta \cong (W_\theta)_o$

(d) $W_r = \epsilon_o W_\theta \phi(\eta_1)$ where $\eta_1 = \frac{r\theta-\delta}{\delta_1}$

} outside the blade boundary layer (Region II)

(e) No net radial mass efflux at any radial location

$$\text{i.e.} \int_o^{\delta} W_r \, r d\theta + \int_{\delta}^{\delta_1} W_r \, r d\theta = 0$$

} for the whole flow region.

the equation (8) can be integrated across half the passage width to provide the following equation

$$0.049 (W_\theta)_o^2 \, \delta \frac{d\epsilon_w}{dR} + (W_\theta)_o^2 \, 0.256 \, \epsilon_w \frac{d\delta}{dR} + \frac{C_f}{2} \cot\beta_t (W_\theta)_o^2 = \frac{(\psi_s)_p - (\psi_s)_s}{4} r_t. \qquad (9)$$

The term on the right hand side can be evaluated from the design flow turning and C_f can be computed from the shear stress correlation obtained for a single helical blade.* If the boundary layer information is available (i.e. ϵ_w and δ), $(W_\theta)_o$ can be computed.

---

*This information is contained in a separate report on "Turbulent Boundary layer characteristics on a rotating helical blade" currently under preparation.

The results from this analysis is not yet conclusive in view of the unknown δ, which cannot be evaluated from any of the data available.

4. FUTURE COURSE OF RESEARCH

Experimental investigation of the flow through the four bladed inducer and the investigation of the boundary layer characteristics on a helical blade has been concluded.

The future experimental and analytical investigations are expected to include the following items, but are not necessarily limited to them.

(1) Three Bladed Inducer

The three bladed inducer is ready for experimentation and the flow at the exit will be surveyed, in the near future, using conventional and hot wire probes.

Based on these measurements, one or several attempts will be made to improve the discharge energy and velocity distribution and to decrease the frictional effects on the inducer.

a) By judiciously designed slots in the tip region of the blades.

b) By use of swept blades where the flow direction is not normal to the leading edge. In such a configuration, the radial flow inside the boundary layer on the exposed part of the leading edge is mixed with mainstream more evenly along the radius. This would probably ensure more even distribution of energy and velocity at the exit of the inducer.

It was anticipated in an earlier report that an artificially roughened surface near the leading edge may minimize large radial flows associated with initial lamina length. This method has been tried on the four bladed inducer without any success.

(2) Rotating Helical Channel

In an axial flow inducer the interaction between the pressure and suction surface boundary layers would result in an extremely complicated flow near the tip.

It is planned at this stage to build a helical channel and run the experiments under free stream conditions. The analytical and experimental study of the boundary layers inside such a channel should provide valuable data for developing a theoretical model of the inducer flow. The experimental investigation would not only include mean velocity profile measurement, wall shear stress measurement, but also turbulence qualities such as intensity, correlation coefficient etc. The hot wire and data processing equipment currently under development will be used in combination with a noise free slip ring unit. The latter, it is anticipated, would be a major instrumentation problem. Therefore no prediction is possible regarding the time required for this part of the investigation.

The analytical investigation of the boundary layer characteristics in a helical channel will be undertaken by three different approaches, in order of complexity.

a) Momentum integral method: This investigation must use a relatively simple approximation for this flow including velocity

profiles and wall shear stress. This investigation would follow the approach outlined under "Theoretical Investigation" Item (c).

b) Asymptotic expansion method

c) Numerical solution of the Navier Stokes equation of motion.

REFERENCES

1. Lakshminarayana, B., Semi-Annual Progress Report on Investigations and Analysis of Flow Phenomena in Axial Flow Inducers., NASA Contract NsG 537, May 1968.

2. Ibid, April 1966.

3. Stanitz, J. D., NACA T. Note 2986.

4. McCafferty, H. G., "Errors in Measuring the Fluctuating Flow at the Discharge of an Inducer" M. S. Thesis, Department of Aerospace Engineering, The Pennsylvania State University, June 1967.

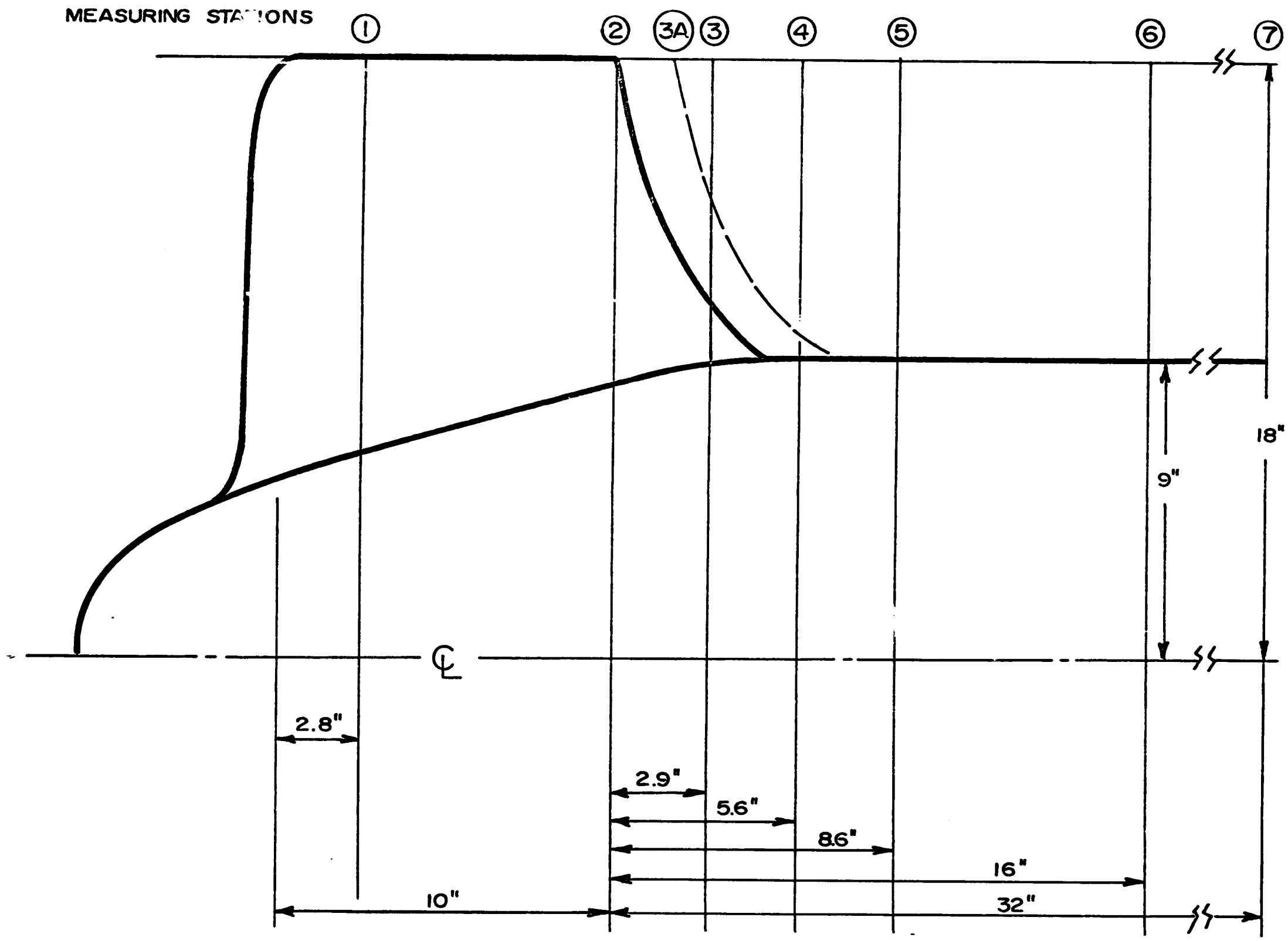

FIGURE I. LOCATION OF THE FLOW MEASURING STATIONS.

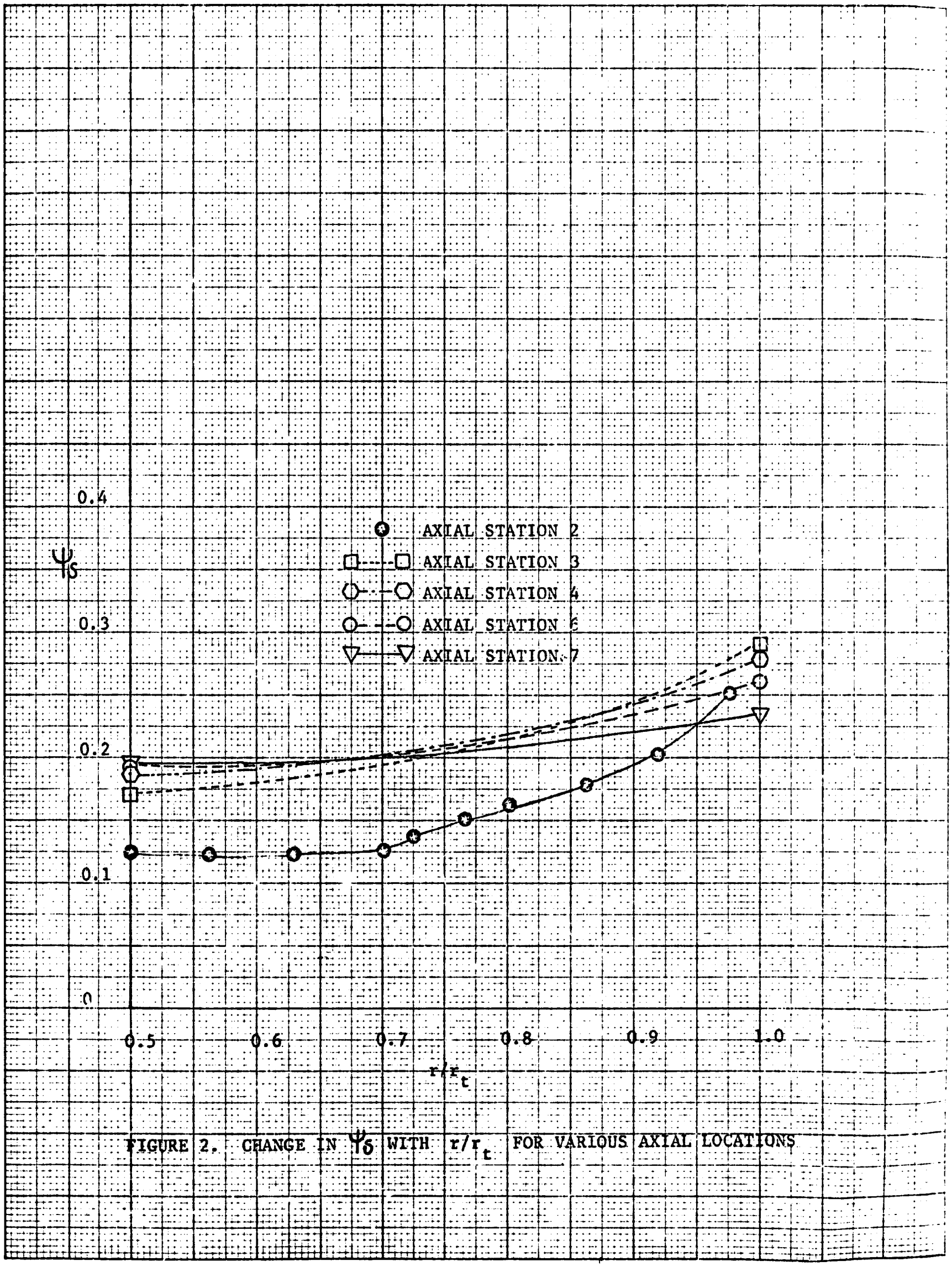

FIGURE 2. CHANGE IN Ψ_S WITH r/r_t FOR VARIOUS AXIAL LOCATIONS

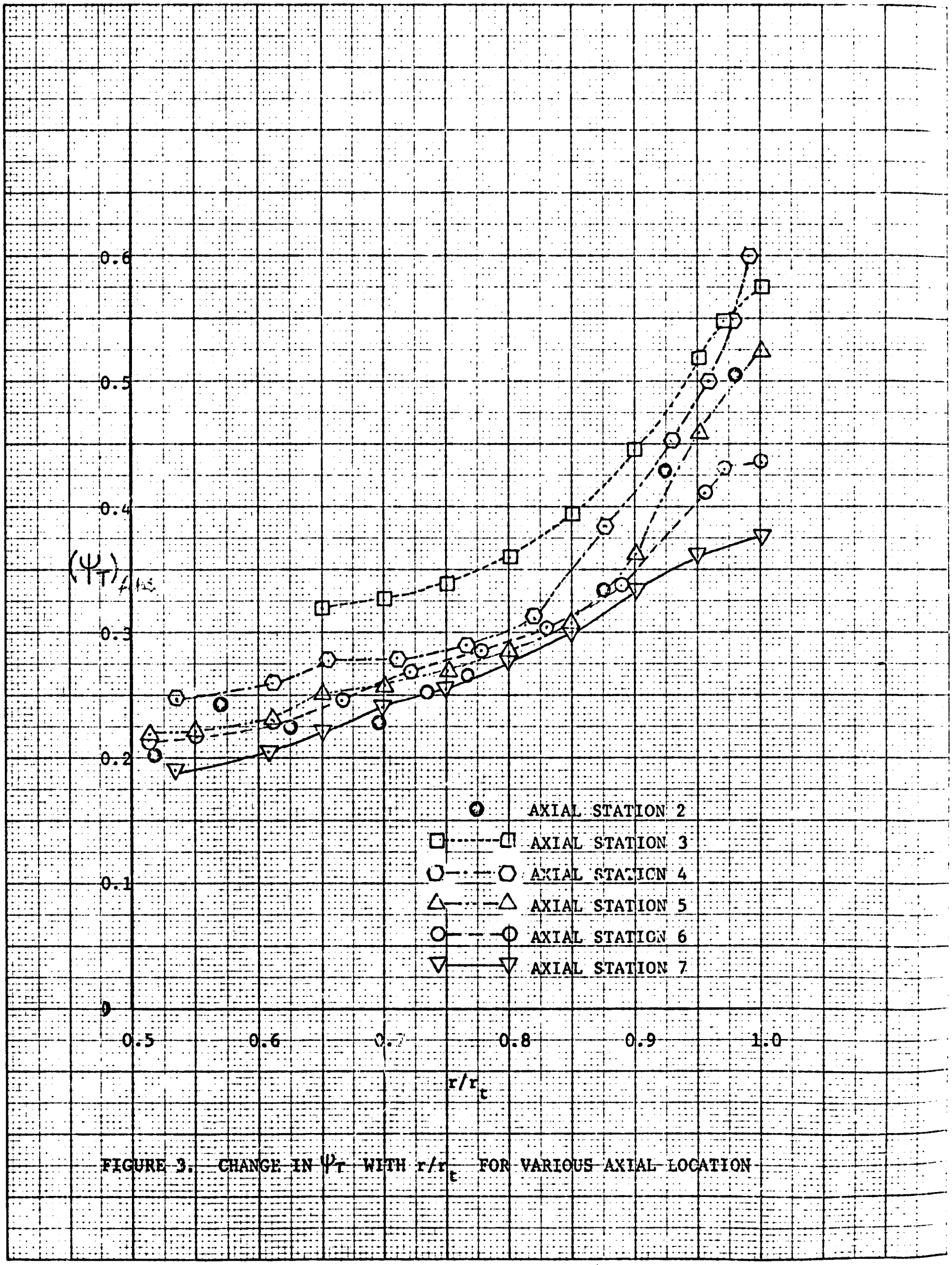

FIGURE 3. CHANGE IN ψ_T WITH r/r_t FOR VARIOUS AXIAL LOCATION

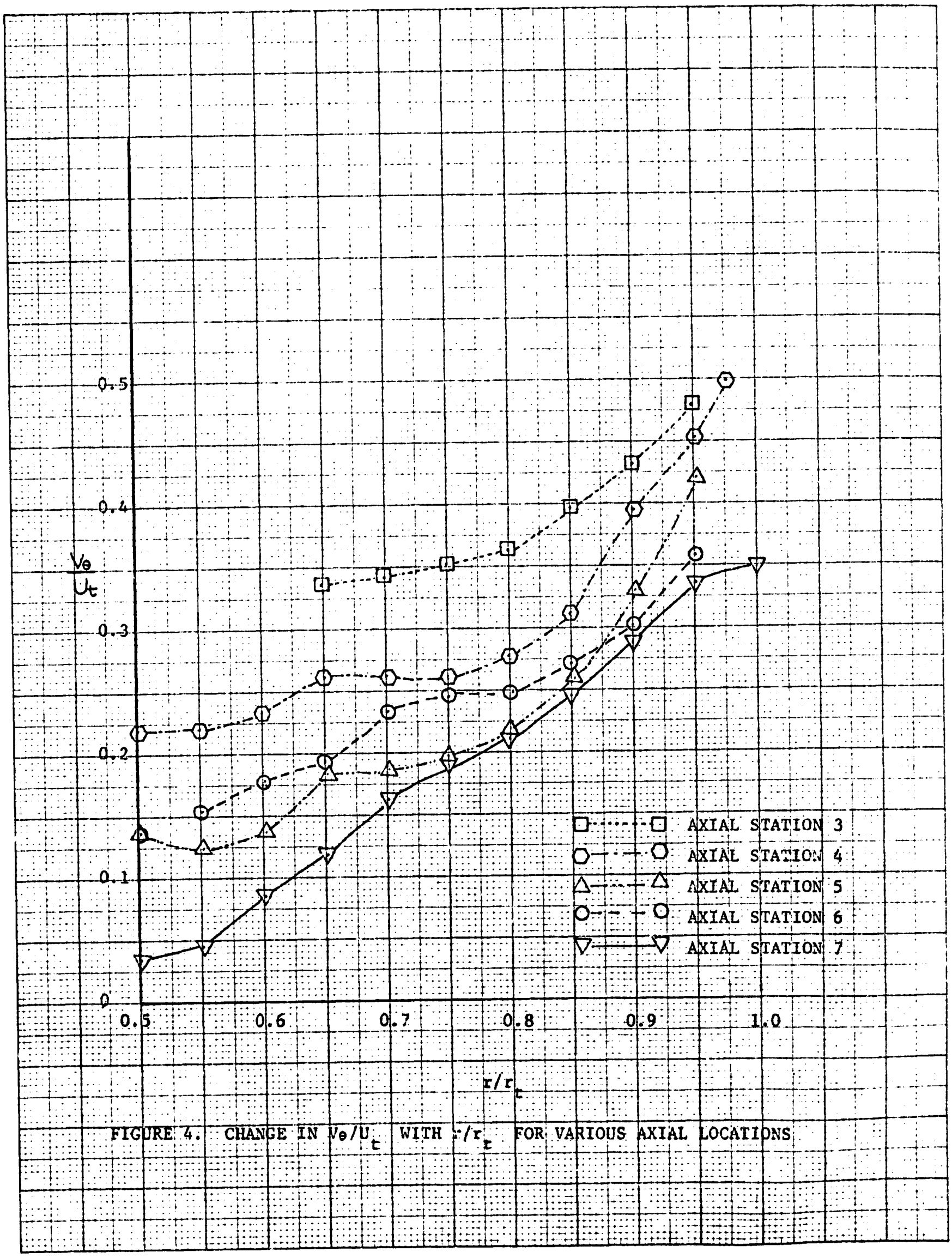

FIGURE 4. CHANGE IN V_θ/U_t WITH r/r_t FOR VARIOUS AXIAL LOCATIONS

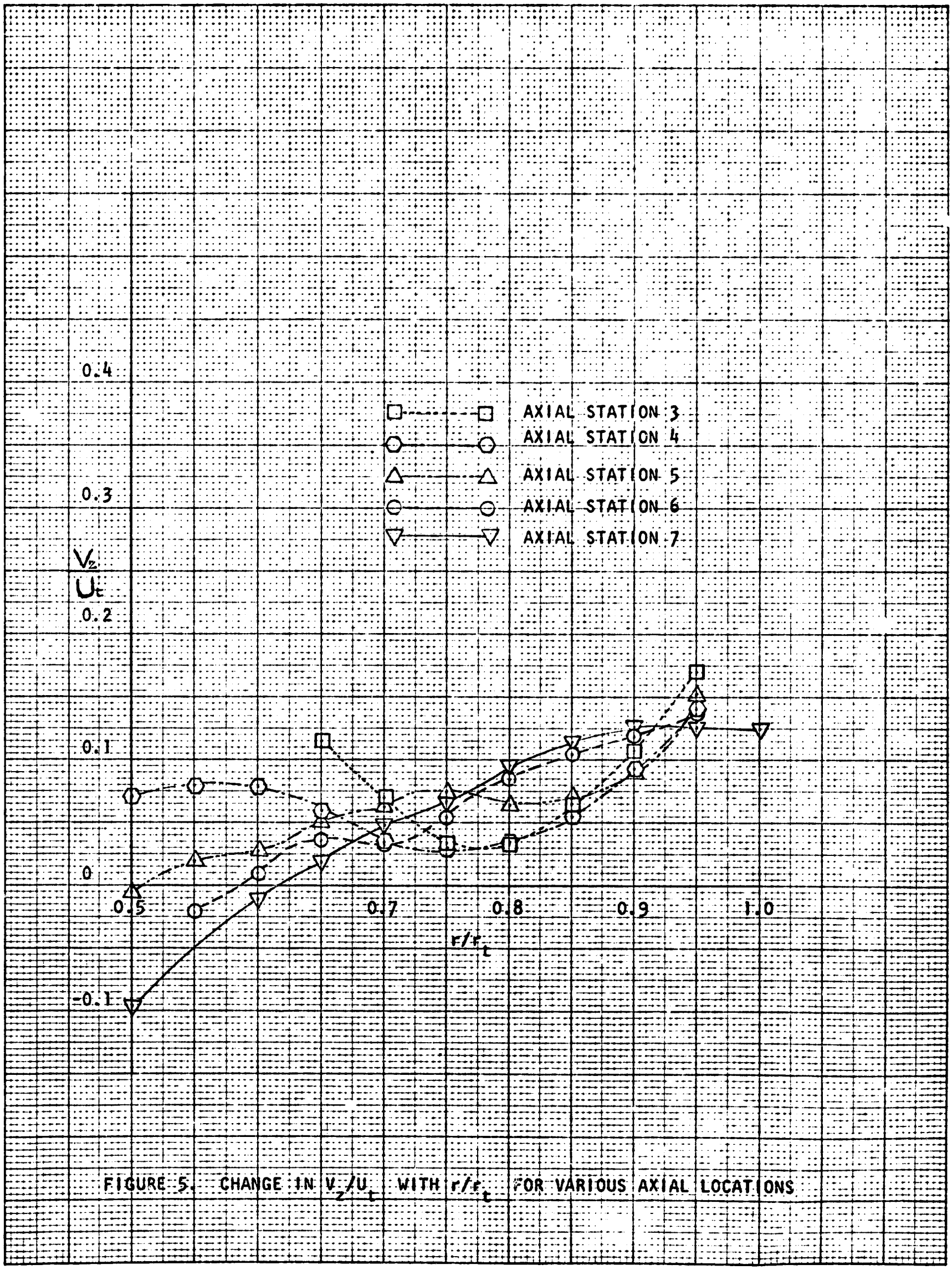

FIGURE 5. CHANGE IN V_z/U_t WITH r/r_t FOR VARIOUS AXIAL LOCATIONS

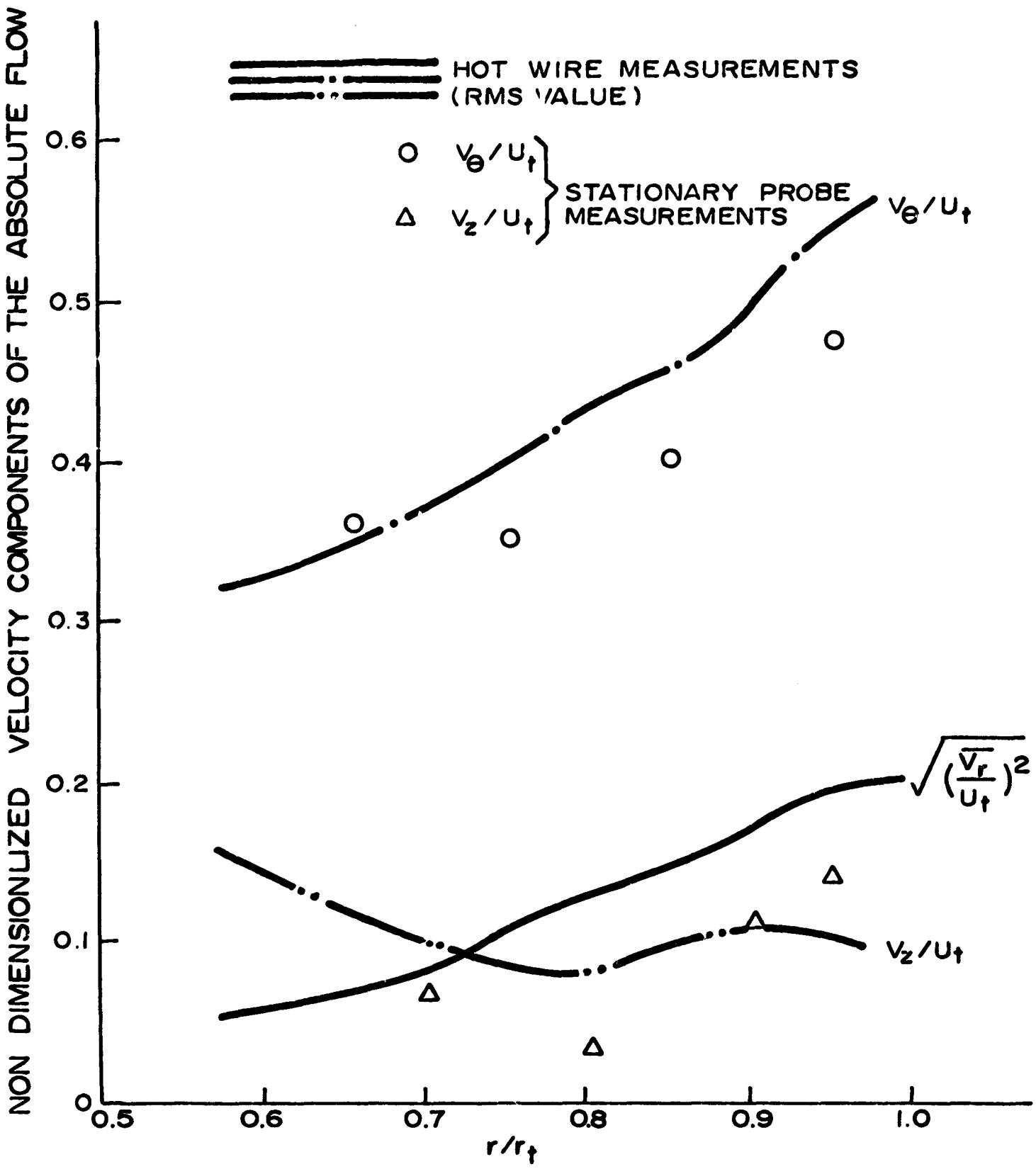

FIGURE 6. COMPARISON OF THE ABSOLUTE VELOCITY COMPONENTS MEASURED BY THE HOT WIRE (RMS VALUE) AND STATIONARY PROBE AT STATION 3A.

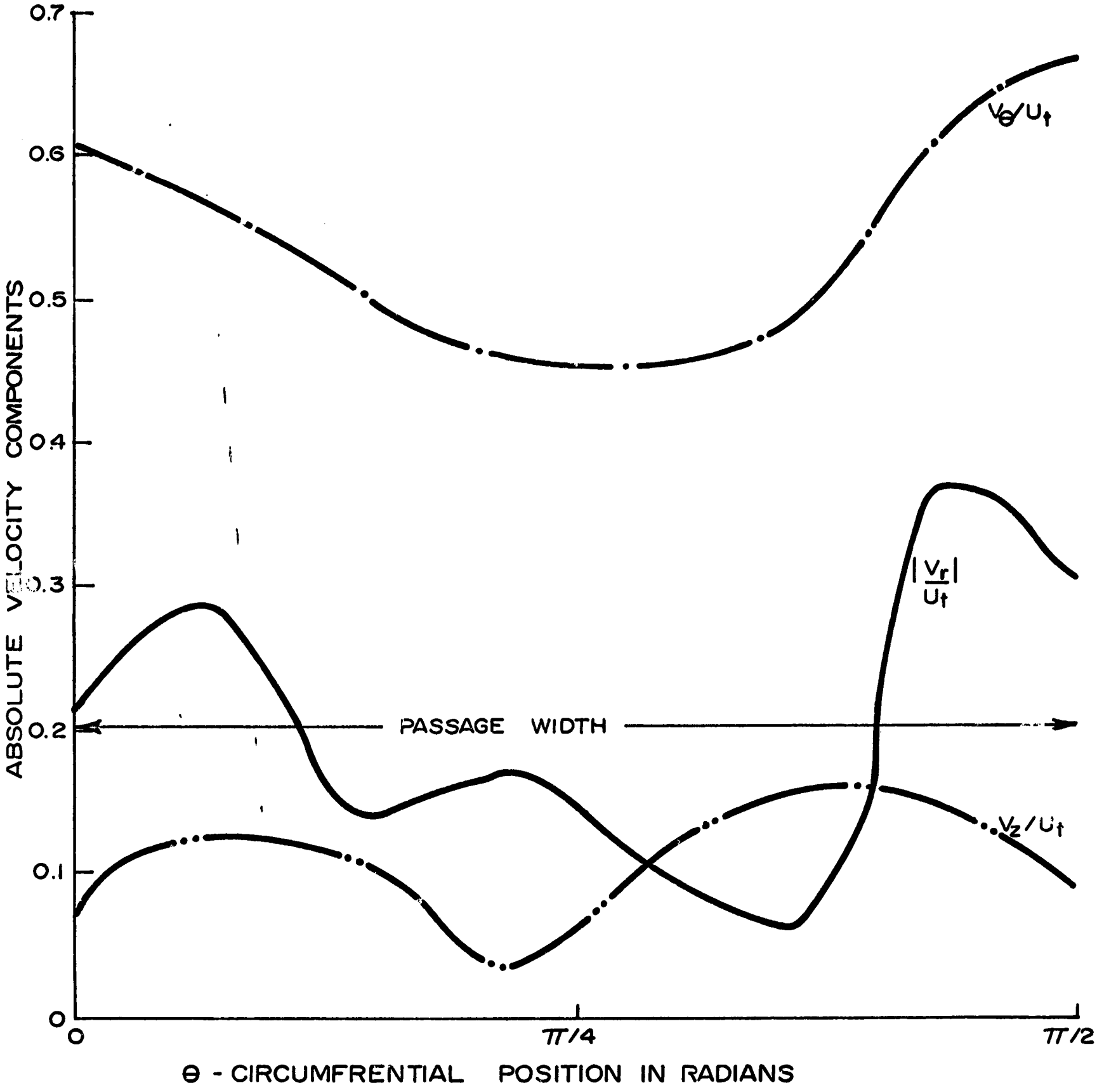

FIGURE 7A. BLADE TO BLADE VARIATION OF THE ABSOLUTE FLOW VELOCITIES DERIVED FROM THE HOT WIRE MEASUREMENTS AT STATION 3A (R = 0.935).

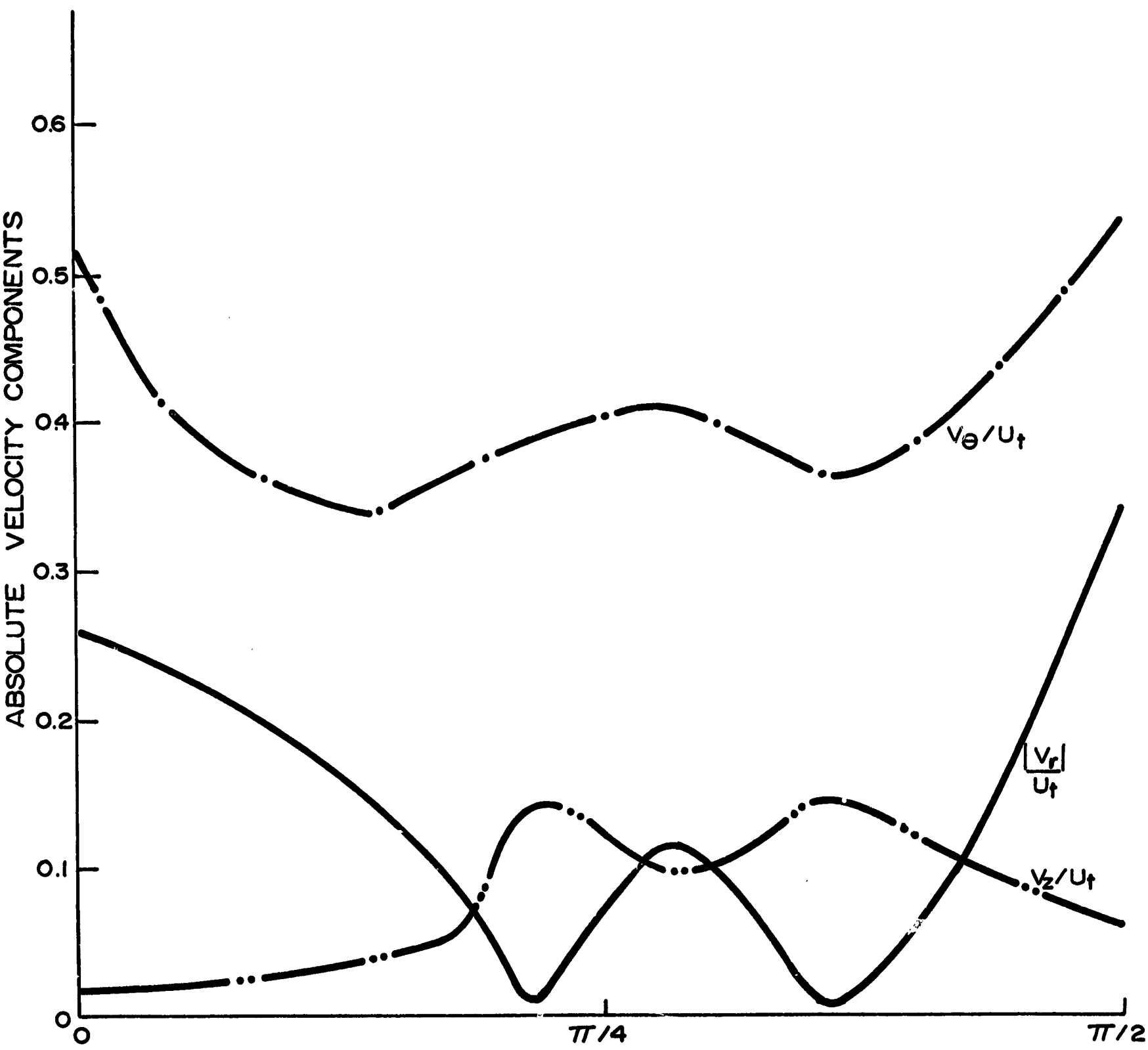

FIGURE 7B. BLADE TO BLADE VARIATION OF THE ABSOLUTE FLOW VELOCITIES DERIVED FROM THE HOT WIRE MEASUREMENTS AT STATION 3A (R = 0.77).

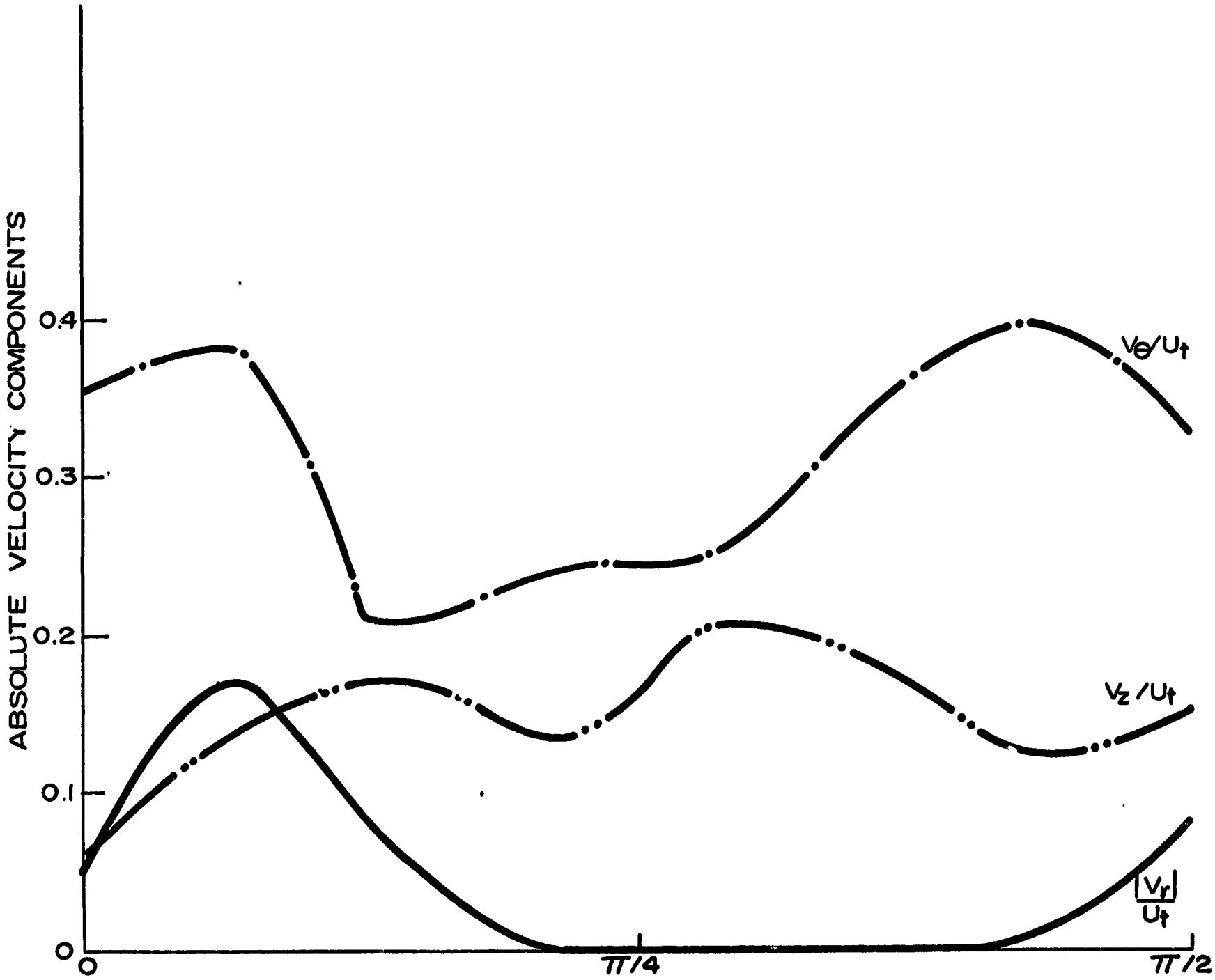

FIGURE 7C. BLADE TO BLADE VARIATION OF THE ABSOLUTE FLOW VELOCITIES DERIVED FROM THE HOT WIRE MEASUREMENTS AT STATION 3A (R = 0.55).

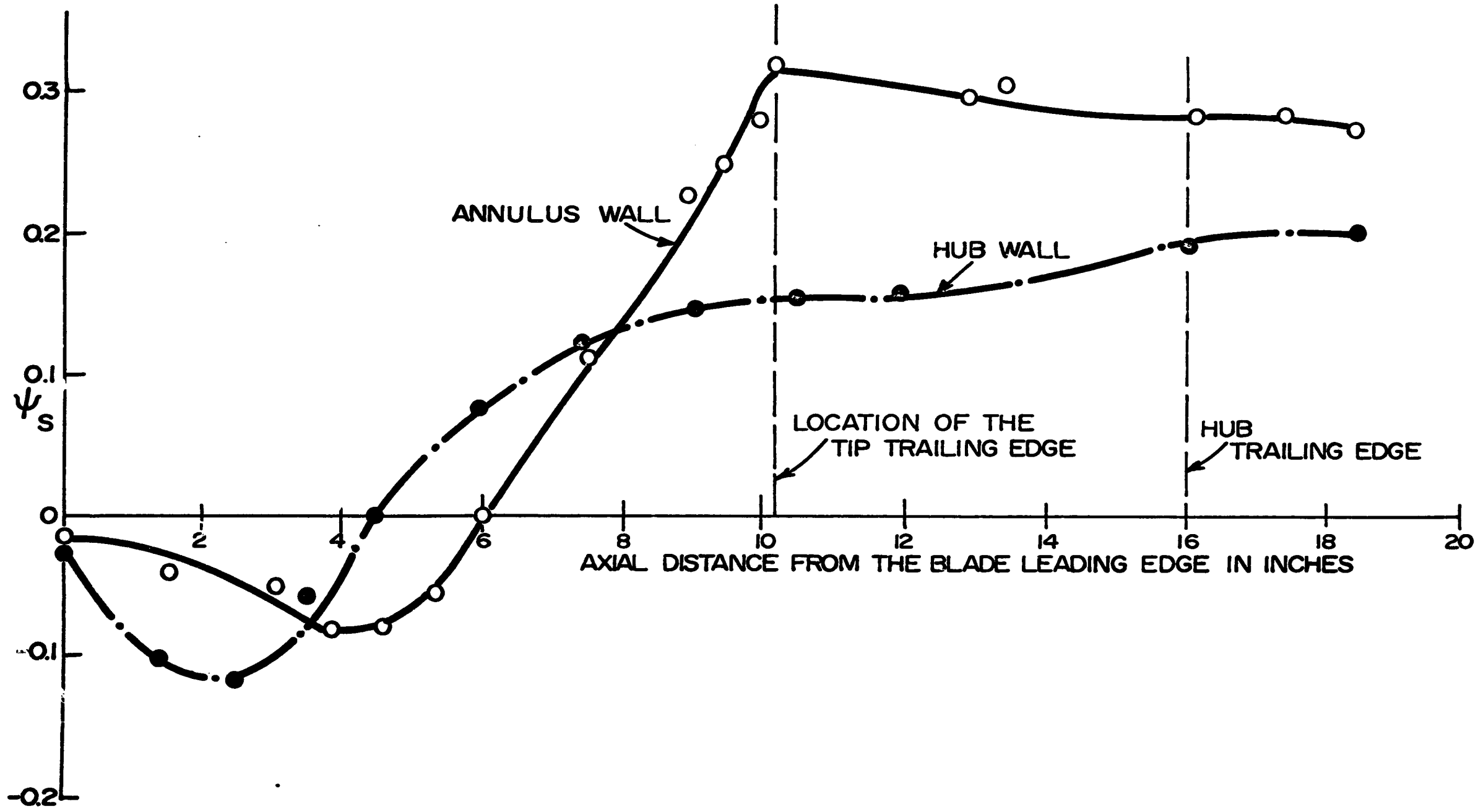

FIGURE 8. ANNULUS WALL AND HUB STATIC PRESSURE.

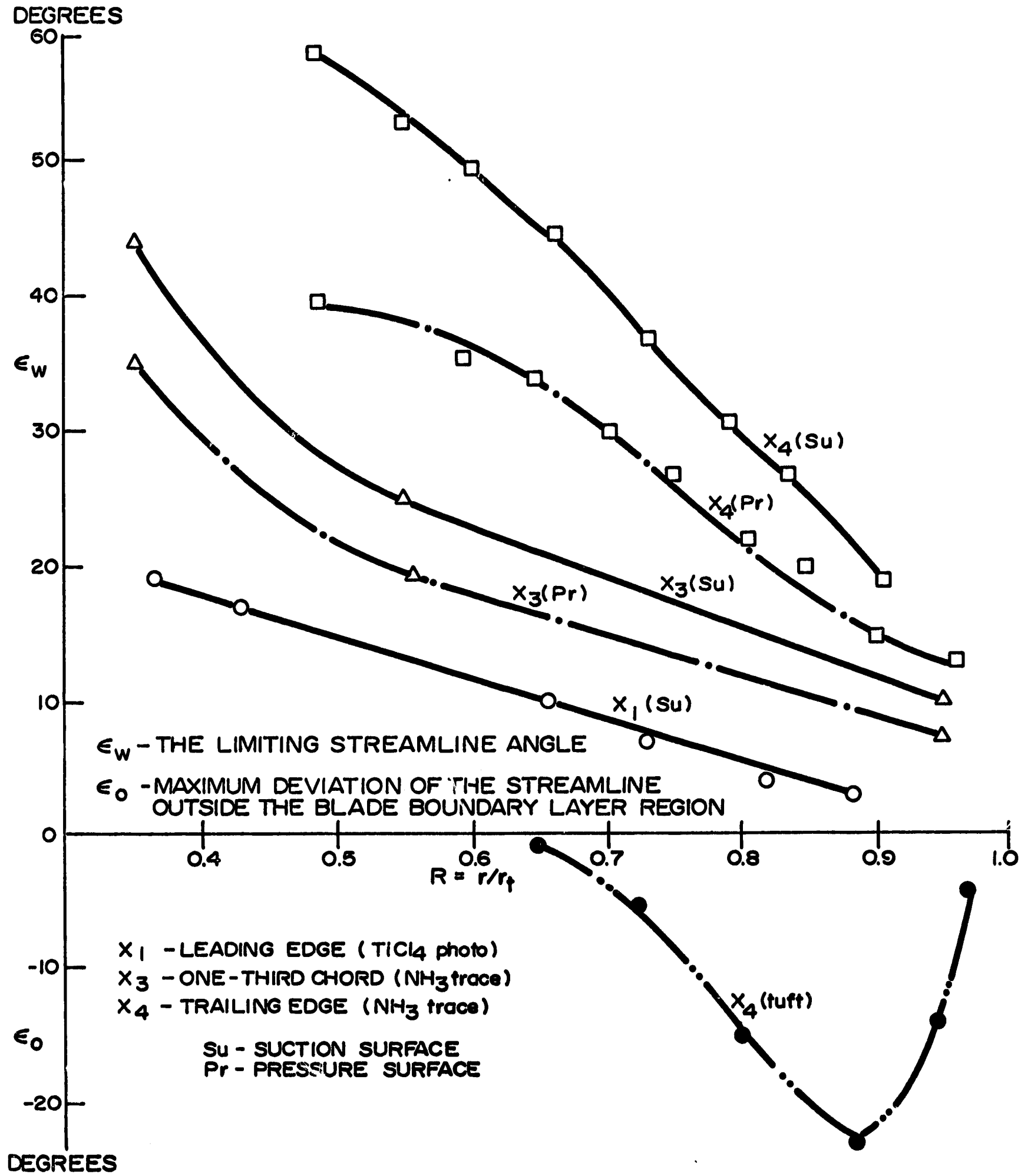

FIGURE 9. RADIAL VARIATION OF THE ANGLES ϵ_w (AT THE BLADE SURFACE) AND ϵ_o (OUTSIDE THE BLADE BOUNDARY LAYER) AT VARIOUS CHORDWISE LOCATION.

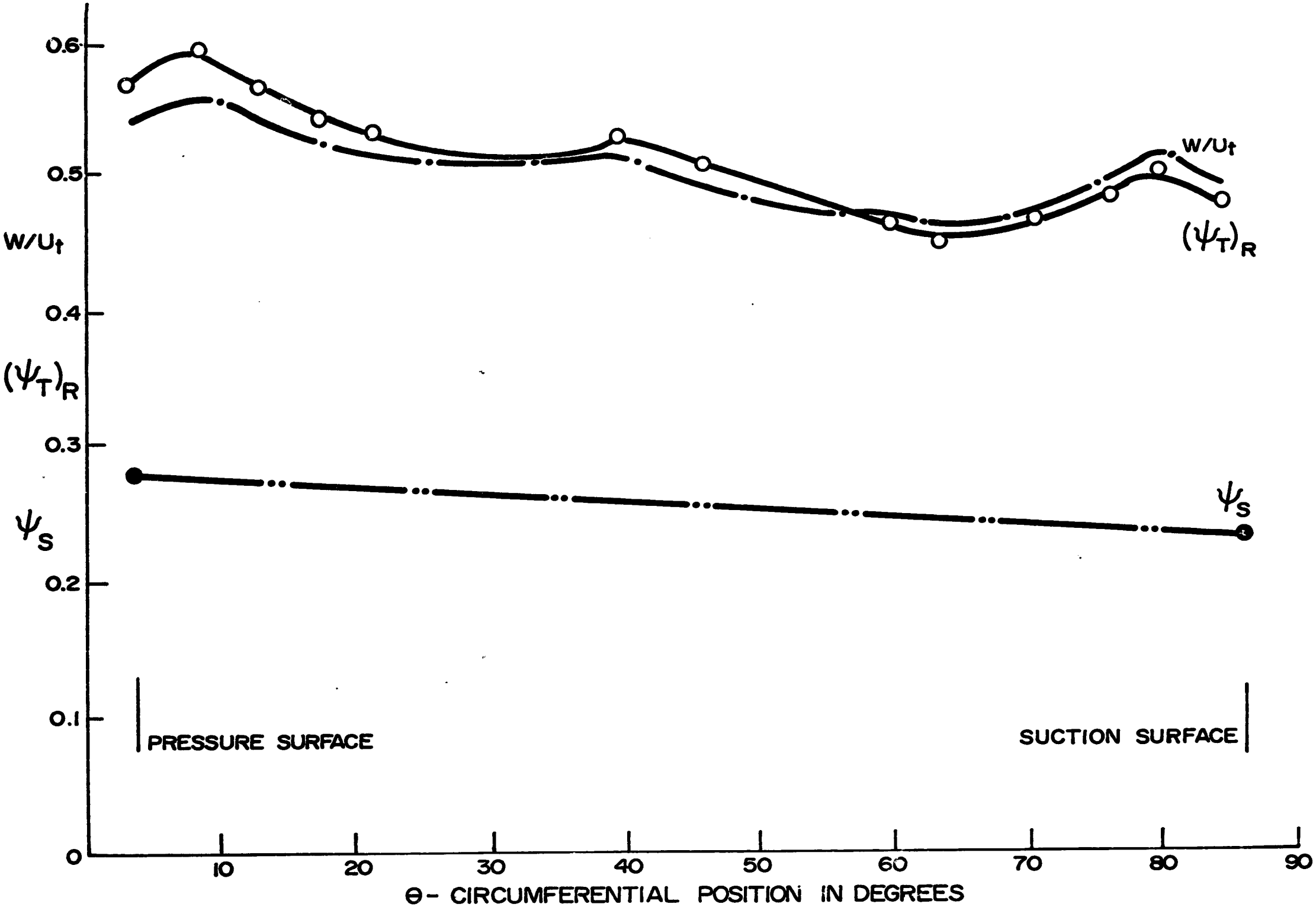

FIGURE 10A. BLADE TO BLADE VARIATION OF STAGNATION PRESSURE COEFFICIENT $(\psi_T)_R$, STATIC PRESSURE COEFFICIENT (ψ_S), AND RESULTANT VELOCITY (W/U_t) OF THE RELATIVE FLOW AT STATION 2 (R = 0.982).

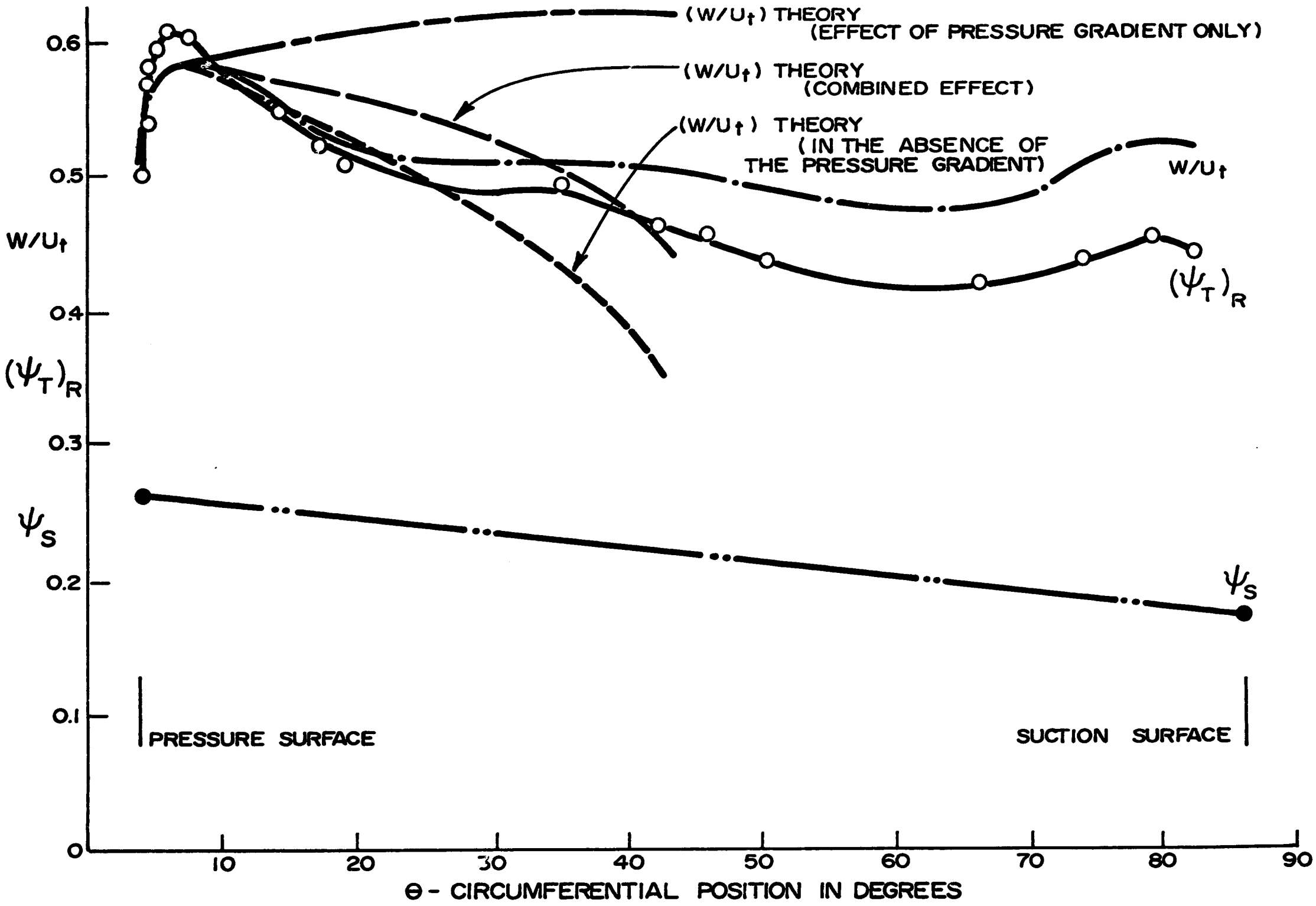

FIGURE 10B. BLADE TO BLADE VARIATION OF STAGNATION PRESSURE COEFFICIENT $(\psi_T)_R$, STATIC PRESSURE COEFFICIENT (ψ_S), AND RESULTANT VELOCITY (W/U_t) OF THE RELATIVE FLOW AT STATION 2 ($R = 0.925$).

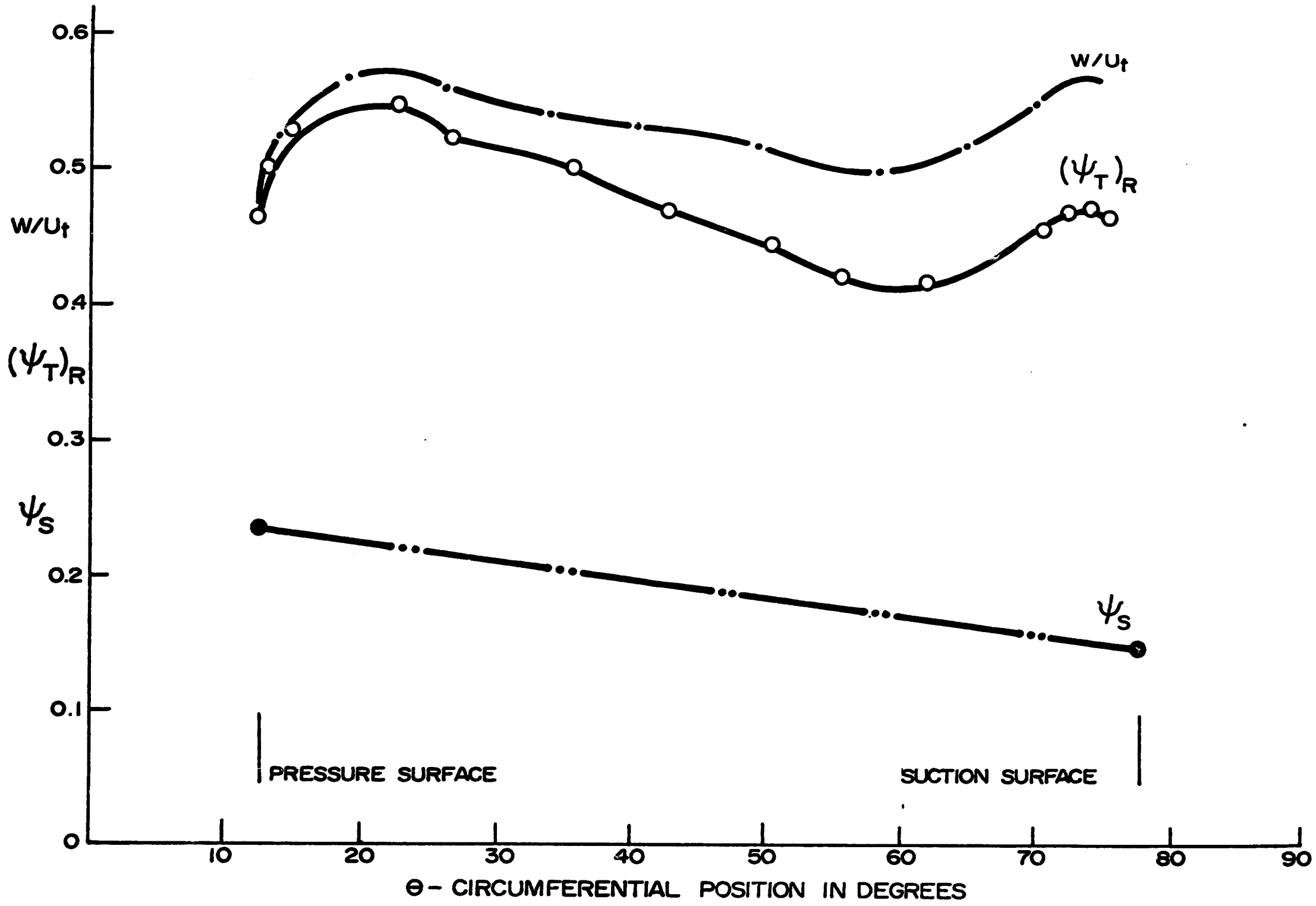

FIGURE 10C. BLADE TO BLADE VARIATION OF STAGNATION PRESSURE COEFFICIENT $(\psi_T)_R$, STATIC PRESSURE COEFFICIENT (ψ_S), AND RESULTANT VELOCITY (W/U_t) OF THE RELATIVE FLOW AT STATION 2 (R=0.872).

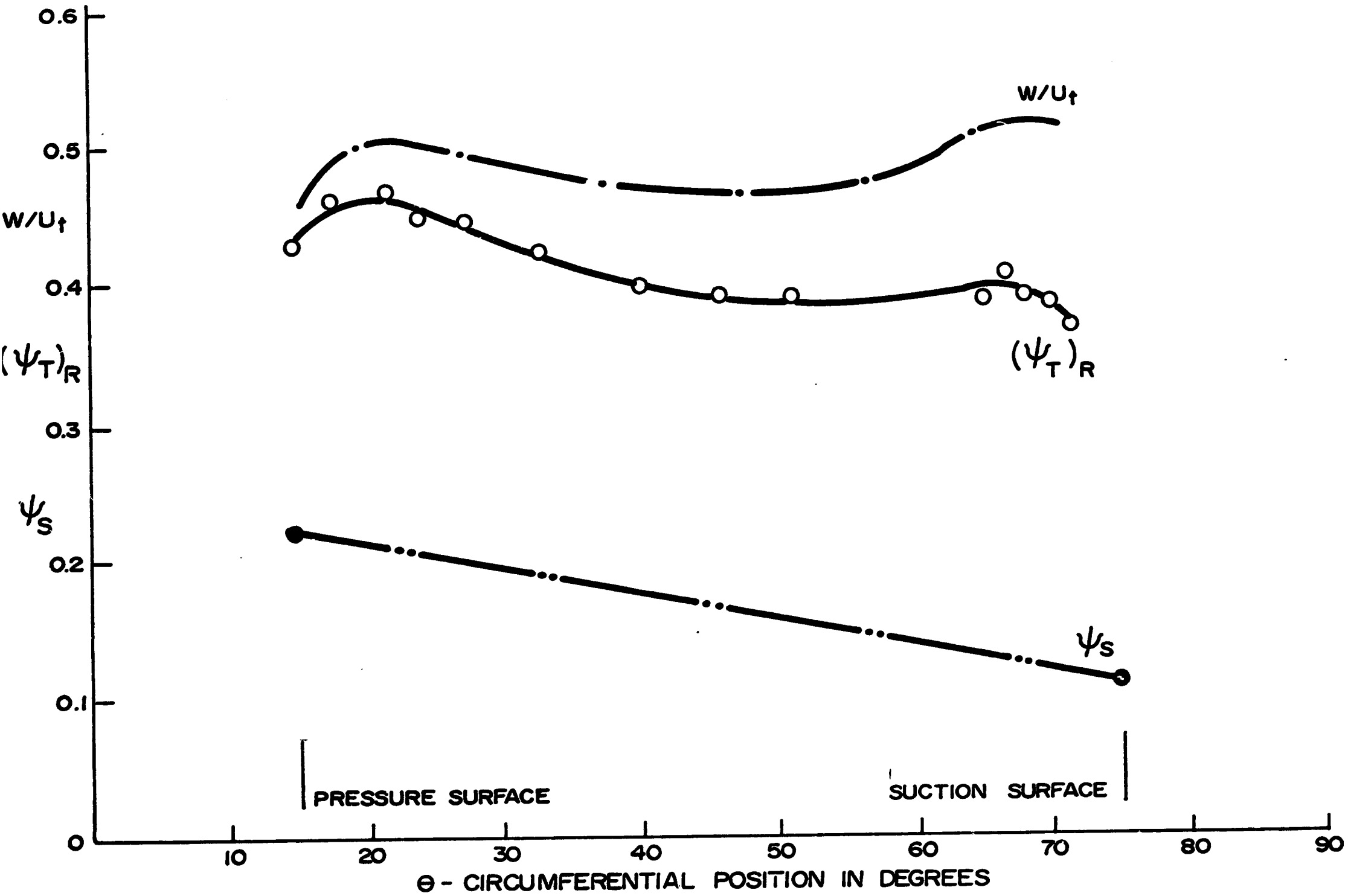

FIGURE 10D. BLADE TO BLADE VARIATION OF STAGNATION PRESSURE COEFFICIENT $(\psi_T)_R$, STATIC PRESSURE COEFFICIENT (ψ_S), AND RESULTANT VELOCITY (W/U_t) OF THE RELATIVE FLOW AT STATION 2 (R=0.815).

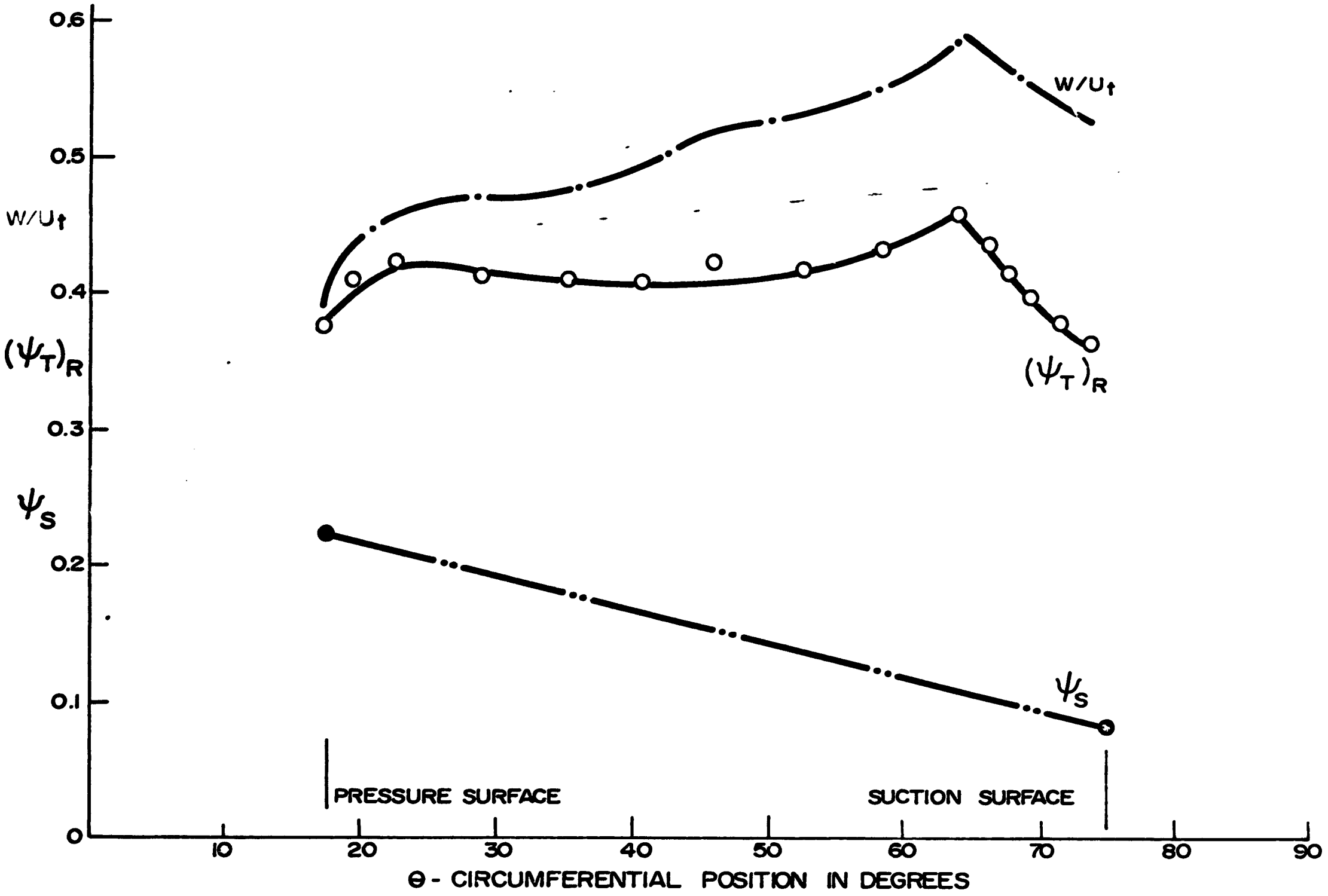

FIGURE 10E. BLADE TO BLADE VARIATION OF STAGNATION PRESSURE COEFFICIENT $(\Psi_T)_R$, STATIC PRESSURE COEFFICIENT (Ψ_S), AND RESULTANT VELOCITY (W/U_t) OF THE RELATIVE FLOW AT STATION 2 (R=0.761).

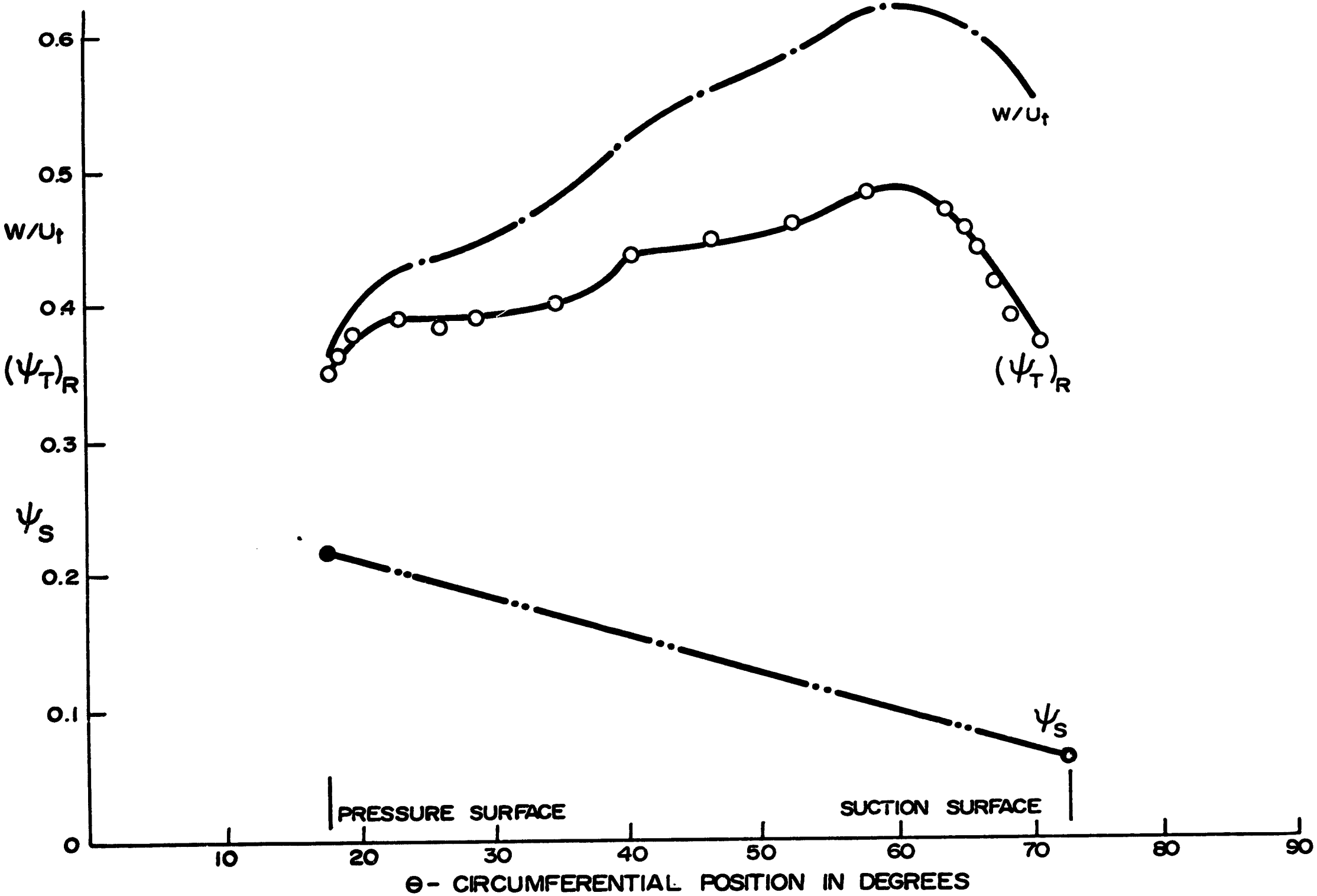

FIGURE 10F. BLADE TO BLADE VARIATION OF STAGNATION PRESSURE COEFFICIENT $(\psi_T)_R$, STATIC PRESSURE COEFFICIENT (ψ_S), AND RESULTANT VELOCITY (W/U_t) OF THE RELATIVE FLOW AT STATION 2 (R=0.735).

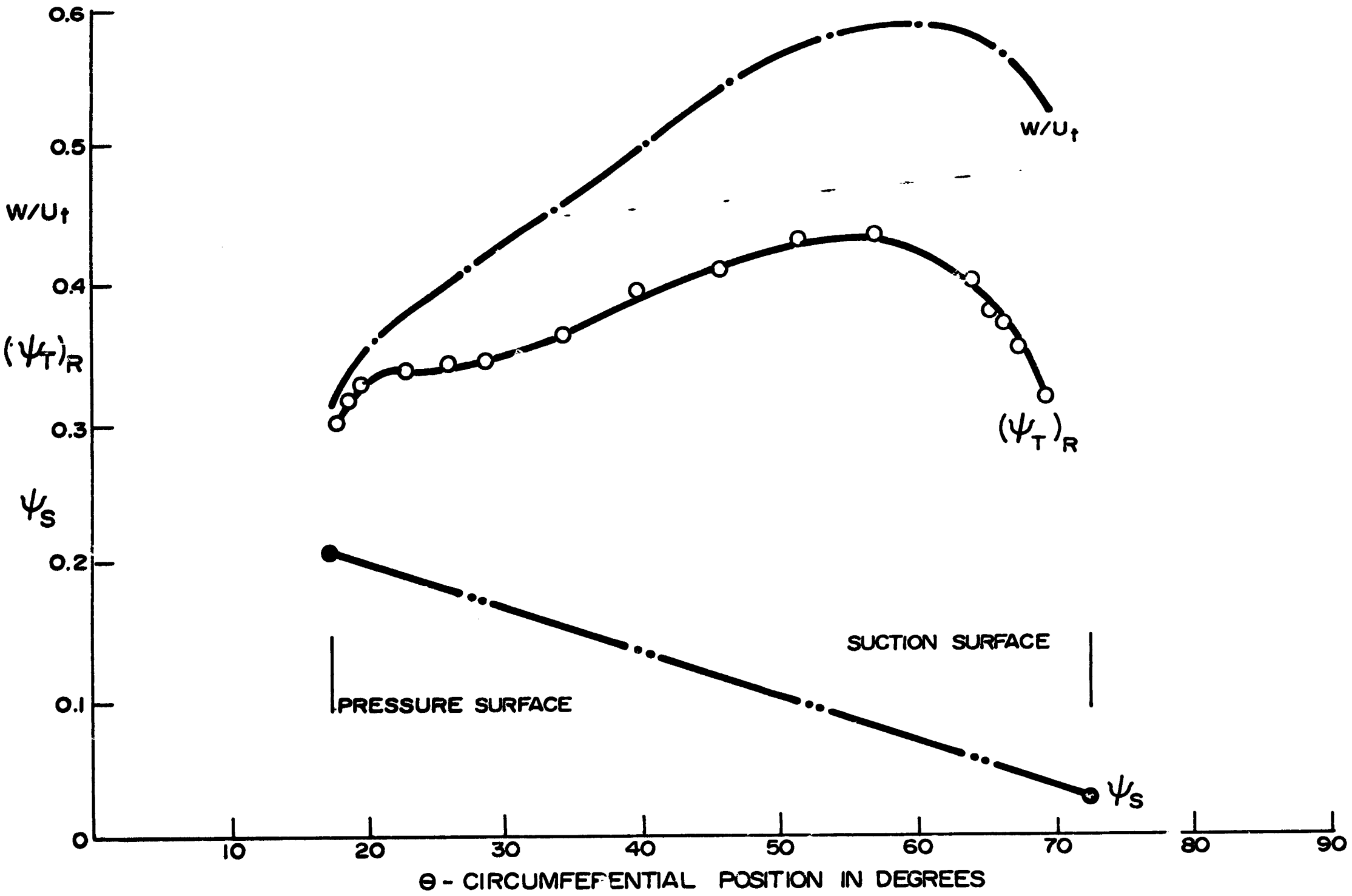

FIGURE 10G. BLADE TO BLADE VARIATION OF STAGNATION PRESSURE COEFFICIENT $(\psi_T)_R$, STATIC PRESSURE COEFFICIENT (ψ_S), AND RESULTANT VELOCITY (W/U_t) OF THE RELATIVE FLOW AT STATION 2 (R=0.690).

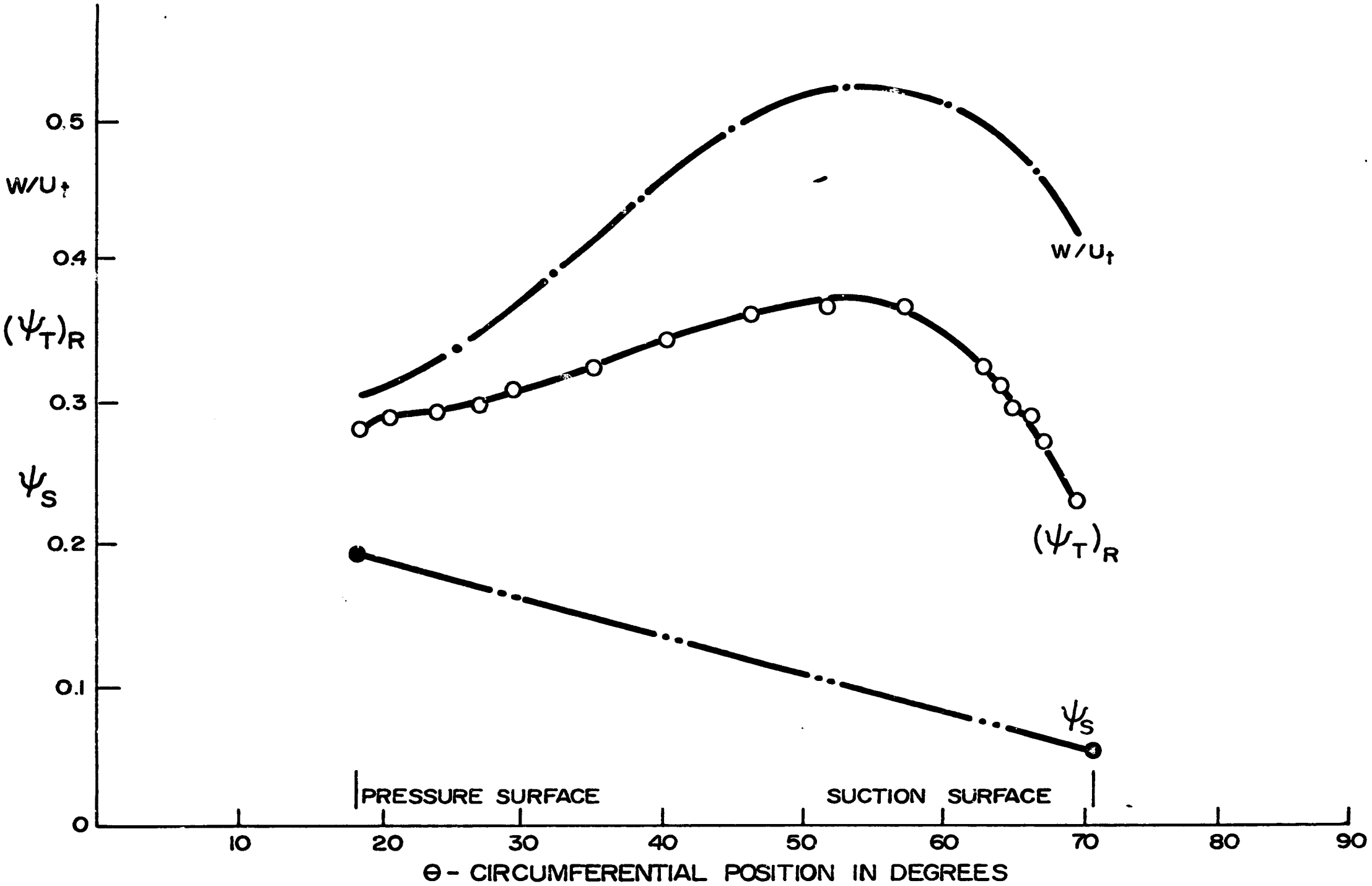

FIGURE 10H. BLADE TO BLADE VARIATION OF STAGNATION PRESSURE COEFFICIENT $(\psi_T)_R$, STATIC PRESSURE COEFFICIENT (ψ_S), AND RESULTANT VELOCITY (W/U_t) OF THE RELATIVE FLOW AT STATION 2 (R=0.631).

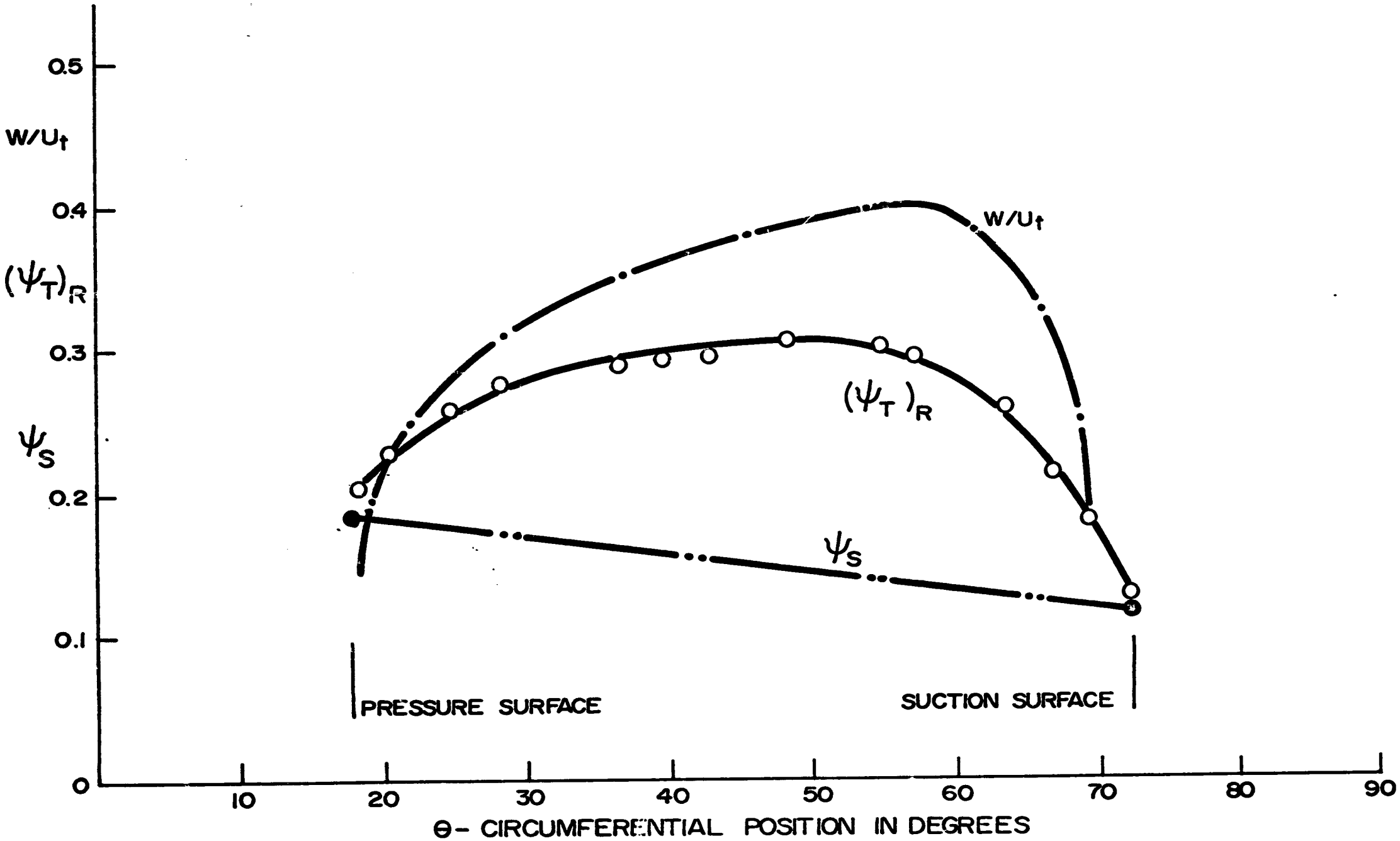

FIGURE 10.1. BLADE TO BLADE VARIATION OF STAGNATION PRESSURE COEFFICIENT $(\psi_T)_R$, STATIC PRESSURE COEFFICIENT (ψ_S), AND RESULTANT VELOCITY (W/U_t) OF THE RELATIVE FLOW AT STATION 2 (R= 0.567).

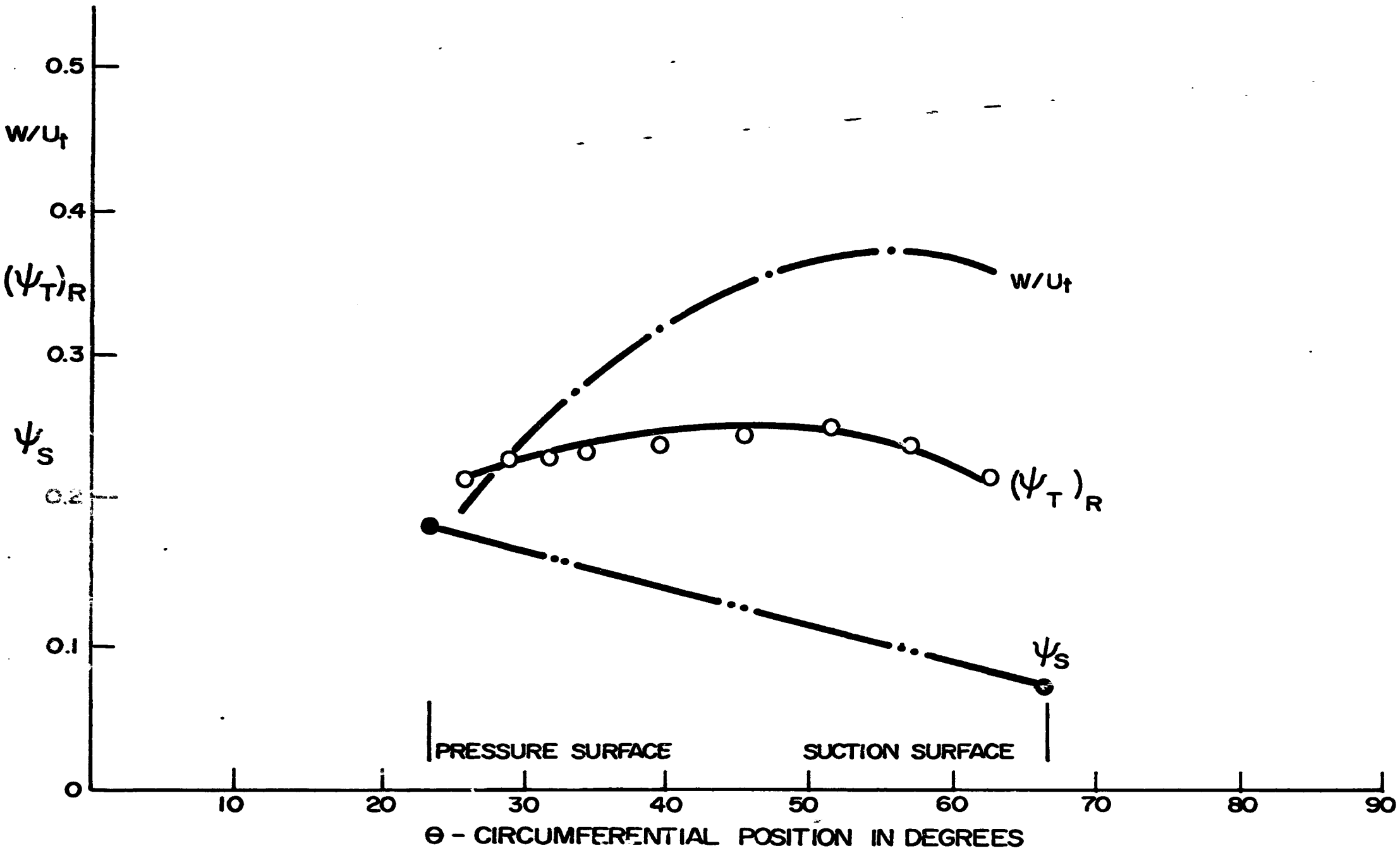

FIGURE 10J. BLADE TO BLADE VARIATION OF STAGNATION PRESSURE COEFFICIENT $(\Psi_T)_R$, STATIC PRESSURE COEFFICIENT (Ψ_S), AND RESULTANT VELOCITY (W/U_t) OF THE RELATIVE FLOW AT STATION 2 (R=0.521).

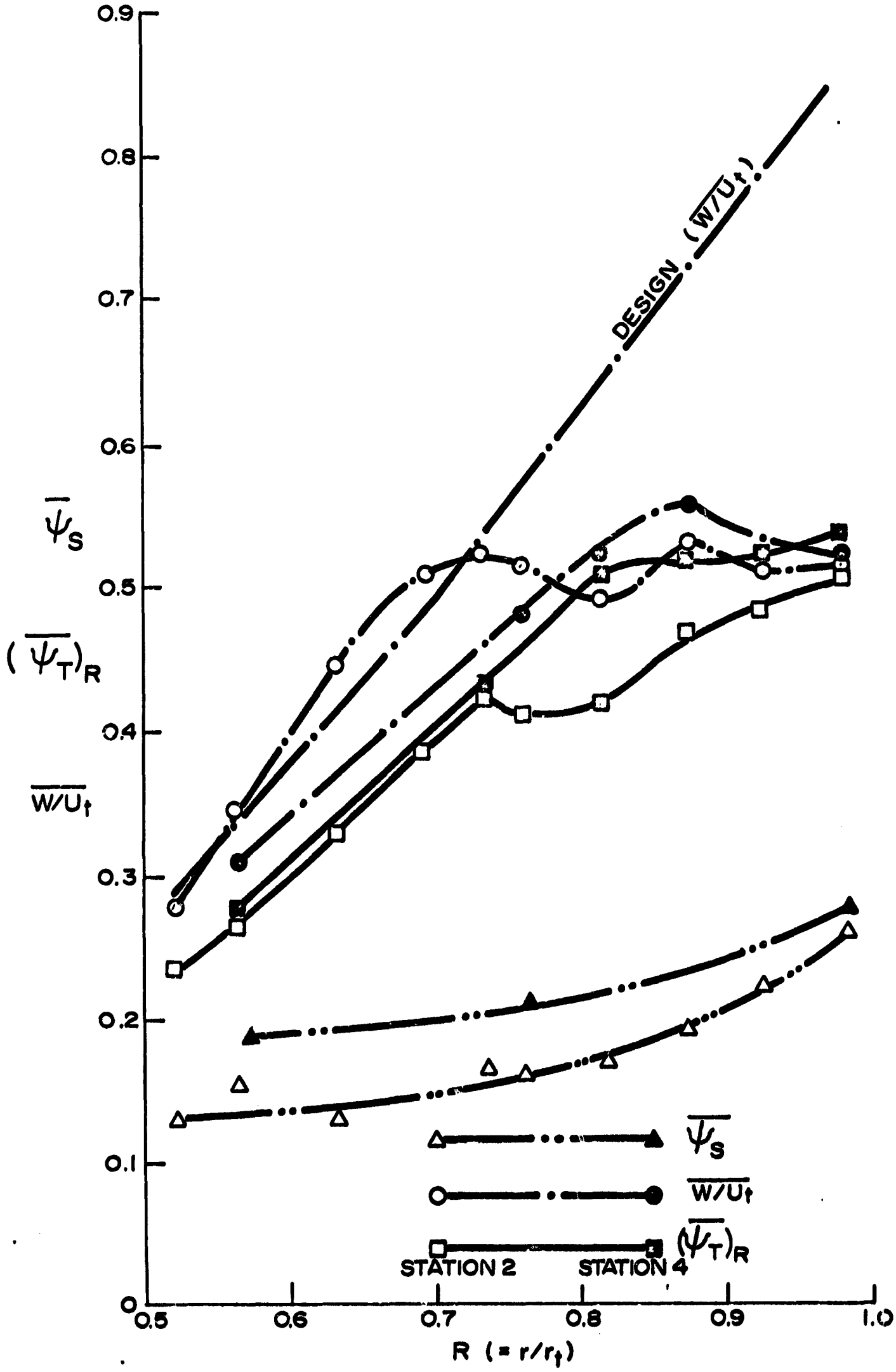

FIGURE 11. RADIAL VARIATION OF THE AVERAGE STAGNATION HEAD COEFFICIENT, STATIC HEAD COEFFICIENT AND VELOCITY OF THE RELATIVE FLOW AT STATIONS 2 AND 4.

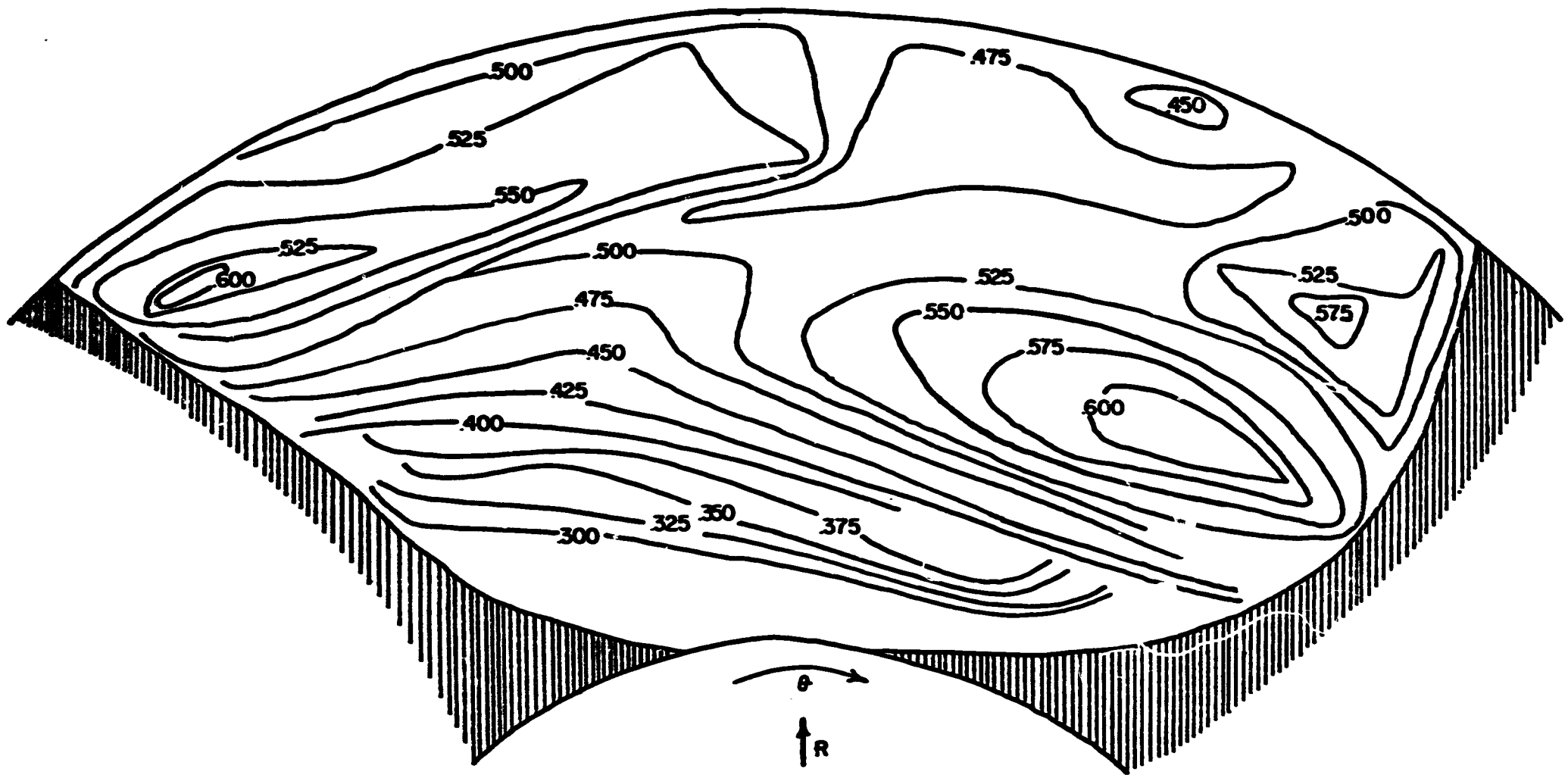

ISO-VELOCITY CONTOURS-W/U_1

AT THE EXIT OF THE INDUCER (STATION 2)

FIGURE 12

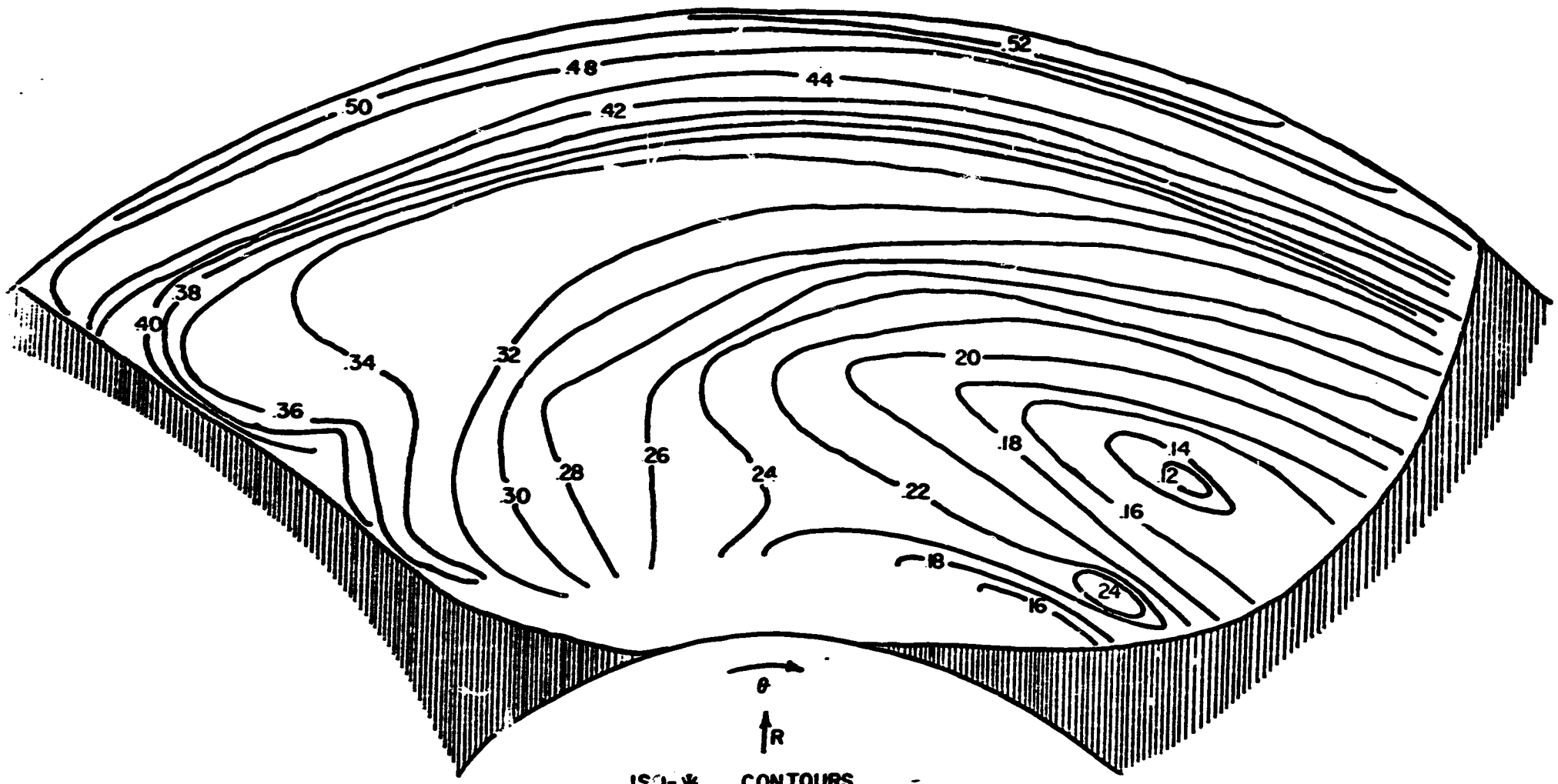

ISO-ψ_{abs} CONTOURS

AT STATION 2

FIGURE 13(a)

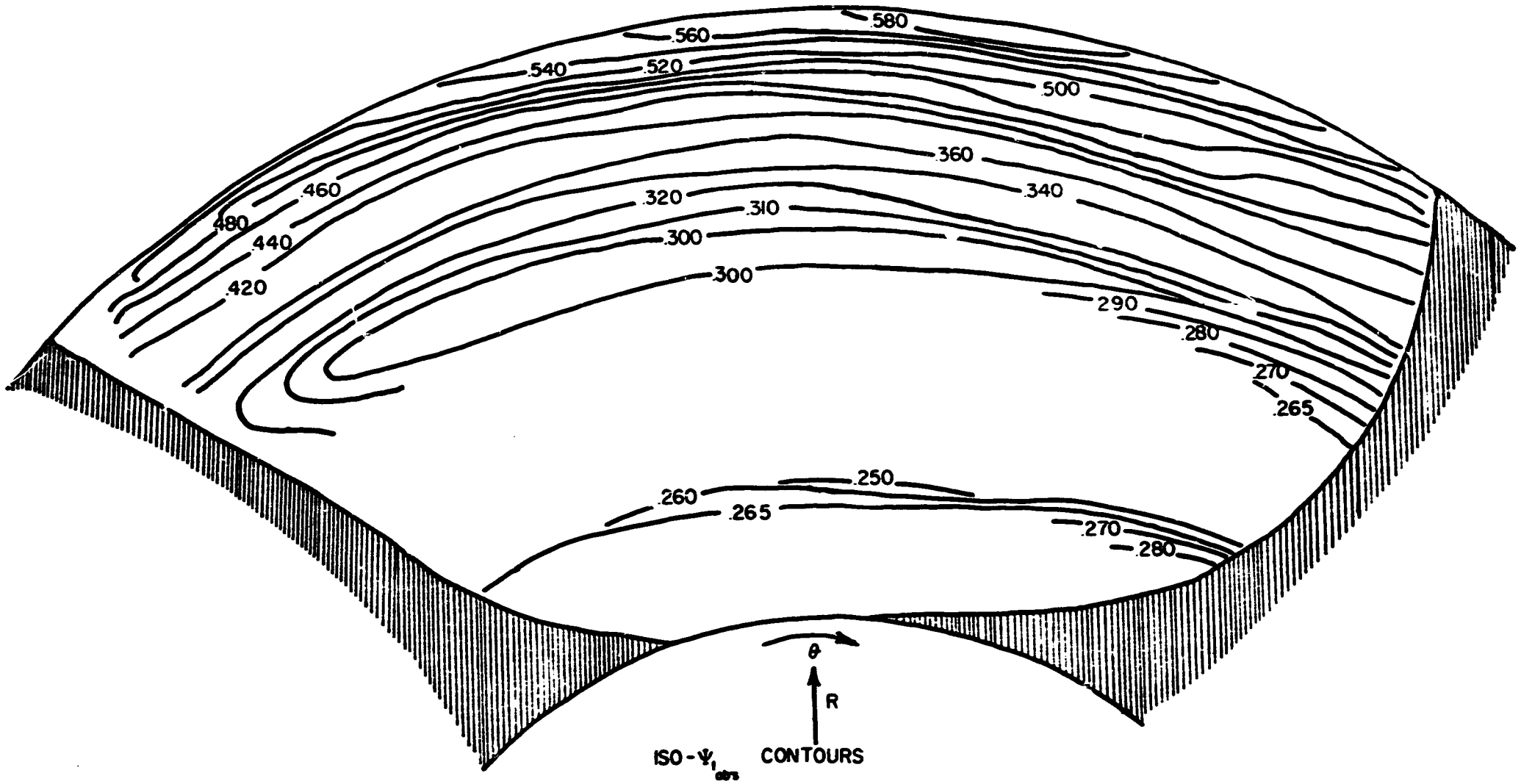
580
560
540
520
500
460
480
440
420
360
340
320
310
300
300
290
280
270
265
250
260
265
270
280
θ
R
ISO-Ψ_{abs} CONTOURS
AT STATION 4

FIGURE 13(b)

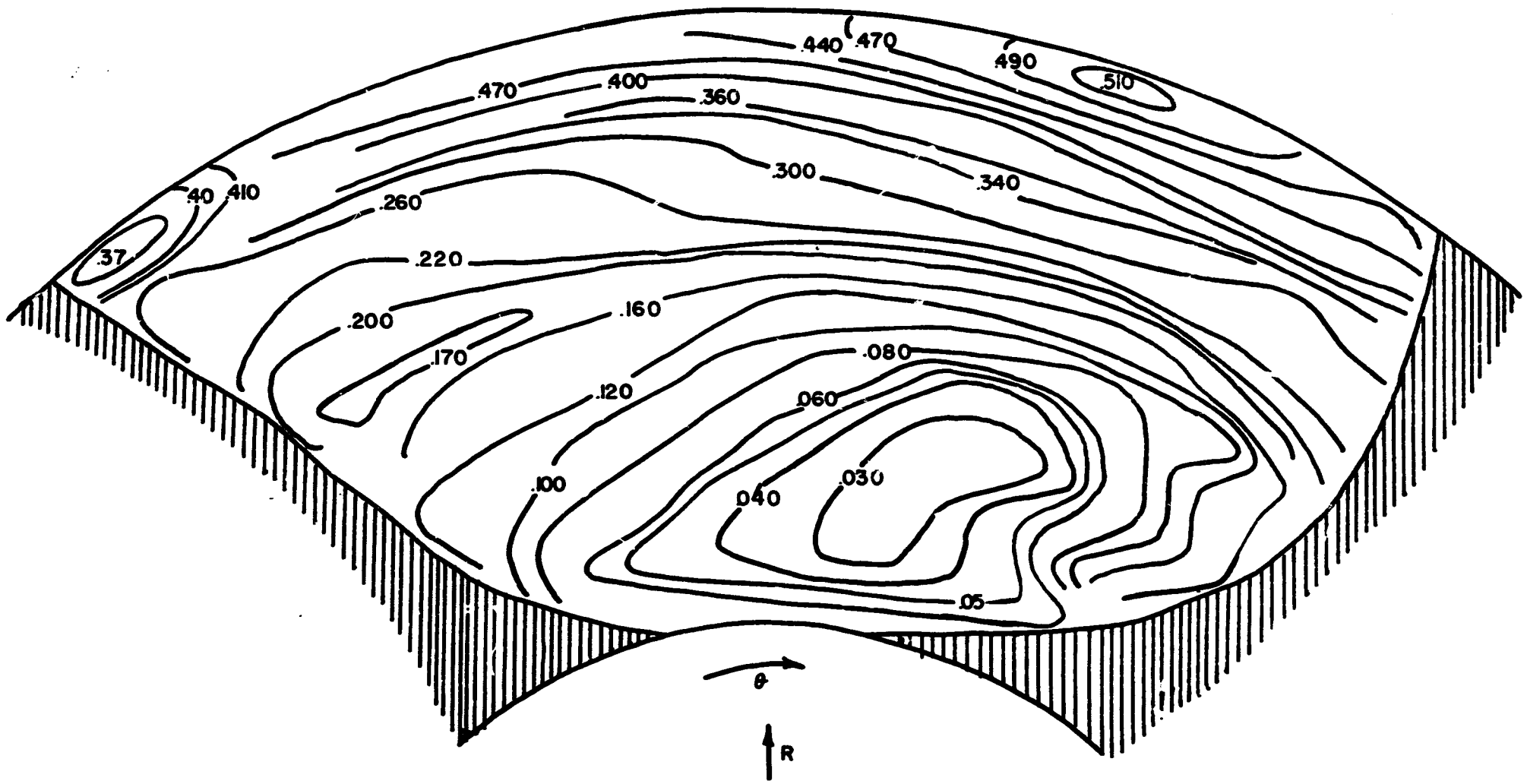

RELATIVE STAGNATION HEAD
LOSS CONTOURS - $(\Psi_1)_{r_{loss}}$

FIGURE 14

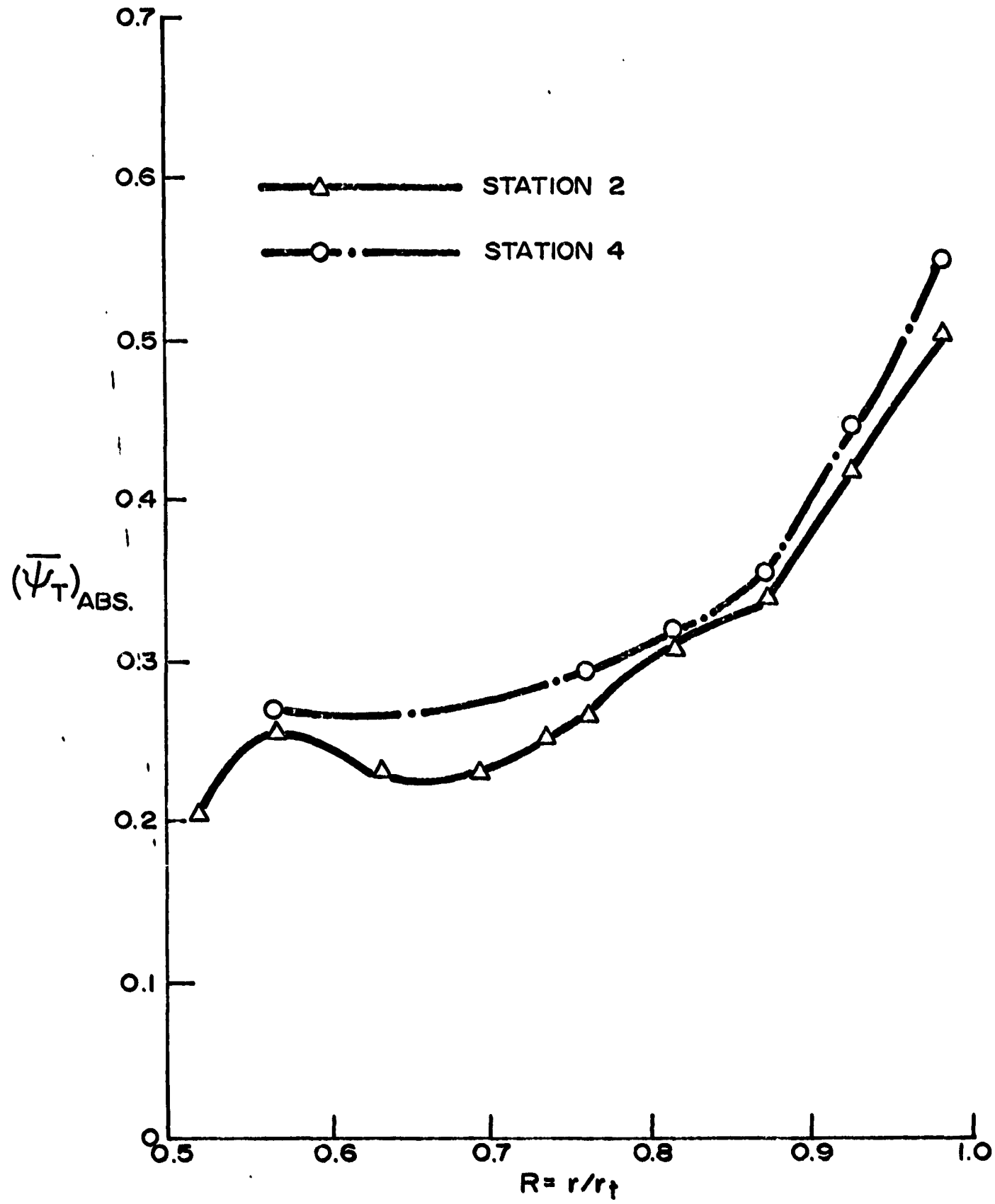

FIGURE 15. RADIAL VARIATION OF THE AVERAGE STAGNATION HEAD COEFFICIENT OF THE ABSOLUTE FLOW AT STATIONS 2 AND 4.

		Tip(r/r_t = 0.975)						
		U/U_t	α	β	V/U_t	V_θ/U_t	V_x/U_t	W/U_t	W_θ/U_t
- - - - -	Design (From simplified radial equilibrium)	0.975	36.0°	5.3°	0.187	0.110	0.080	0.877	0.865
———	Based upon absolute flow measurements	0.975	25.0°	24.0°	0.528	0.478	0.223	0.545	0.497
— - —	Derived from spacial average relative flow measurements	0.975	19.5°	15.0°	0.446	0.421	0.148	0.574	0.554

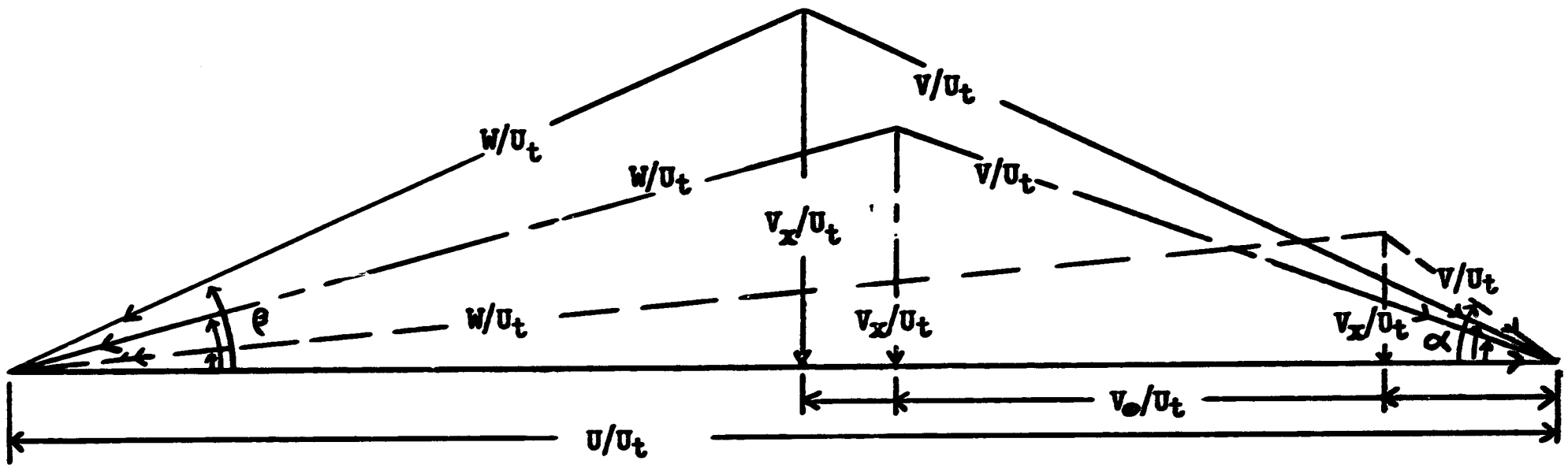

Figure 1.6(a): Comparison of the Design Velocity Triangles with the Velocity Triangles Derived from Relative and Absolute Flow Measurements

station 4 Barry mccafferty (Ref 4)

Tip $r/r_t = 0.975$

		U/U_t	α	β	V/U_t	V_θ/U_t	V_x/U_t	W/U_t
- - - - - -	Desigr	0.975	36°	5.3°	0.187	0.110	0.08	0.865
———	Absolute flow measurements	0.975	19°	20°	0.53	0.5	0.175	0.5
——— · ———	Relative flow measurements (averaged over the passage)	0.975	16°	17.5°	0.53	0.51	0.140	0.49

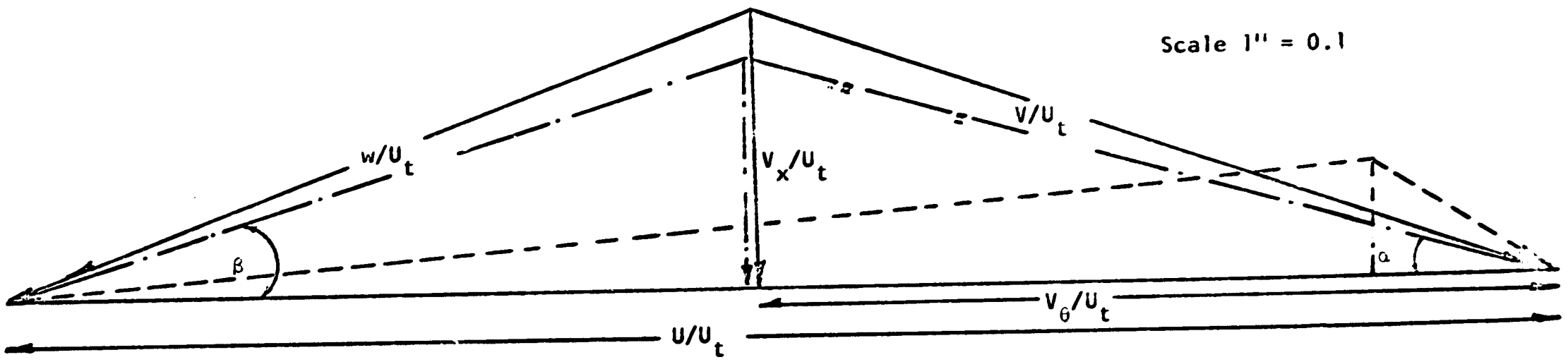

Fig. 16a Revised Comparison of velocity triangles derived from relative and absolute flow measurements $r/r_t = 0.975$, Station 4.

Mid-radius(r/r_t = 0.777)

		U/U_t	α	β	V/U_t	V_θ/U_t	V_x/U_t	W/U_t	W_θ/U_t
- - - - -	Design (From simplified radial equilibrium)	0.777	25.4°	8.0°	0.198	0.179	0.085	0.607	0.598
———	Based upon absolute flow measurements	0.777	32.5°	19.6°	0.330	0.278	0.177	0.529	0.499
— - —	Derived from spanwise average relative flow measurements	0.777	18.0°	8.3°	0.254	0.241	0.078	0.542	0.536

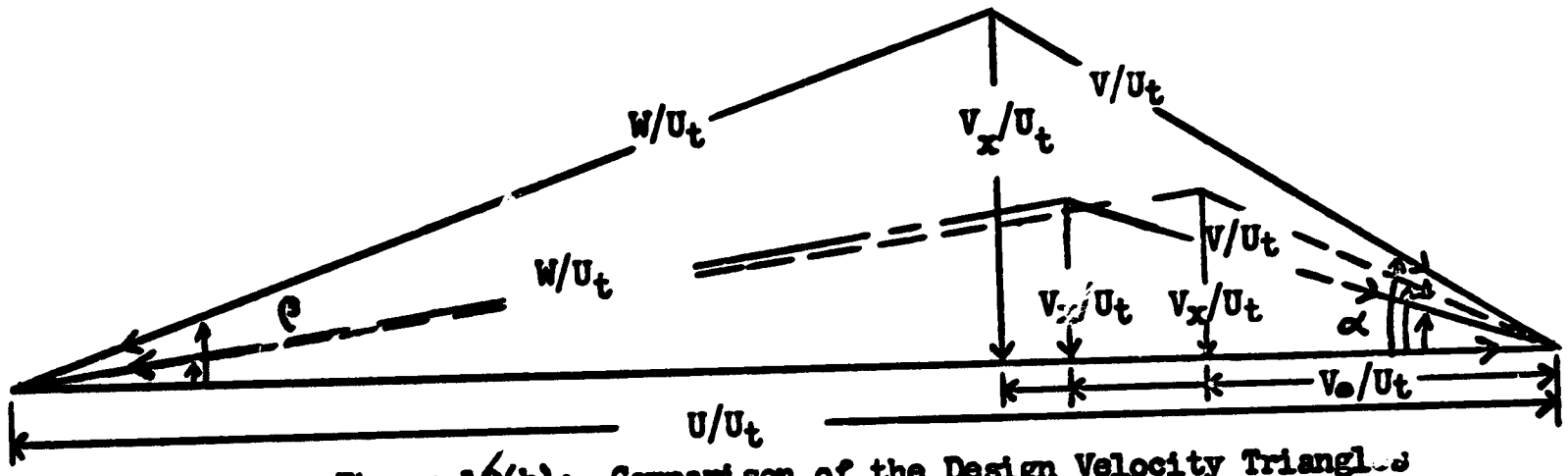

Figure 19(b): Comparison of the Design Velocity Triangles with the Velocity Triangles Derived from Relative and Absolute Flow Measurements Station 4 H.G.McCafferty (Ref 4)

$r/r_t = 0.777$

		U/U_t	α	β	V/U_t	V_θ/U_t	V_x/U_t	w/U_t
— — — —	Design	0.777	25.4°	8.0°	0.198	0.179	0.085	.607
————	Absolute flow measurements	0.777	10.0°	5.0°	0.27	0.265	0.04	.515
—·—	Relative flow measurements (averaged over the passage)	0.777	18.0°	9.0°	0.275	0.260	0.080	.525

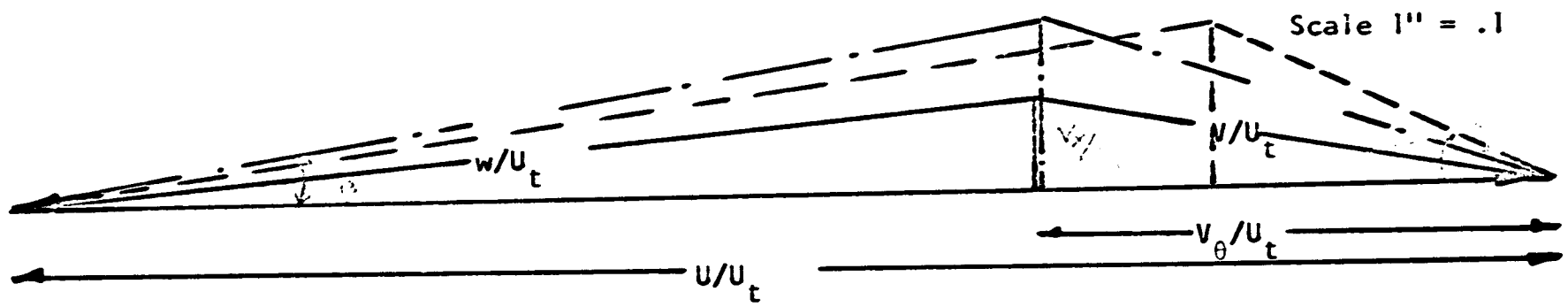

Fig. 16b Revised Comparison of velocity traingles derived from relative and absolute flow measurements $r/r_t = 0.777$, Station 4.

Hub($r/r_t = 0.55$)

	U/U_t	α	β	V/U_t	V_θ/U_t	V_x/U_t	W/U_t	W_θ/U_t
- - - - - Design (From simplified radial equilibrium)	0.55	26°	17.4°	0.239	0.215	0.105	0.351	0.335
——— Based upon absolute flow measurements	0.55	0°	0°	0.161	0.161	0.0	0.389	0.389
— - — Derived from spacial average relative flow measurements	0.55	0°	0°	0.170	.0.170	0.0	0.380	0.380

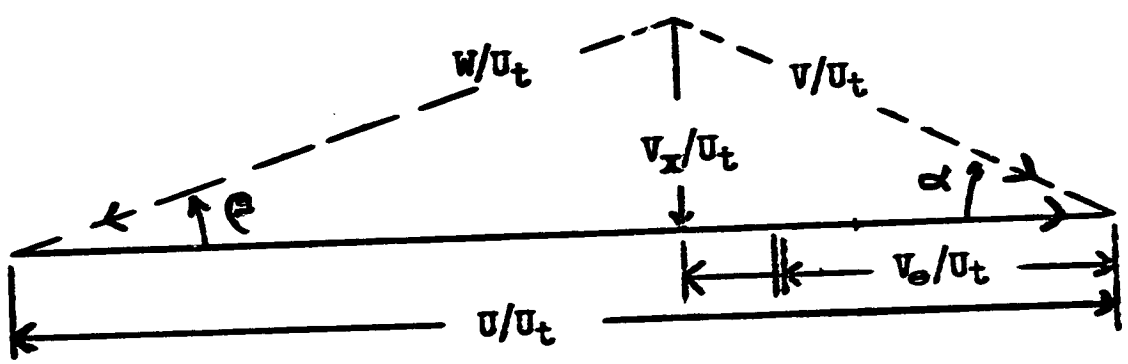

Figure 16(c): Comparison of the Design Velocity Triangles with the Velocity Triangles Derived from Relative and Absolute Flow Measurements
Station 4 -H.G.McCafferty (Ref 4)

HUB $r/r_t = 0.55$

		U/U_t	α	β	V/U_t	V_θ/U_t	V_x/U_t	w/U_t
- - - -	Design	0.55	26°	17.4°	0.24	0.215	0.105	0.351
———	Absolute flow measurement	0.55	22°	15.5°	0.24	0.2125	0.09	0.345
—·—	Relative flow measurement (averaged over the passage)	0.55	25°	16.5°	0.245	0.225	0.100	0.355

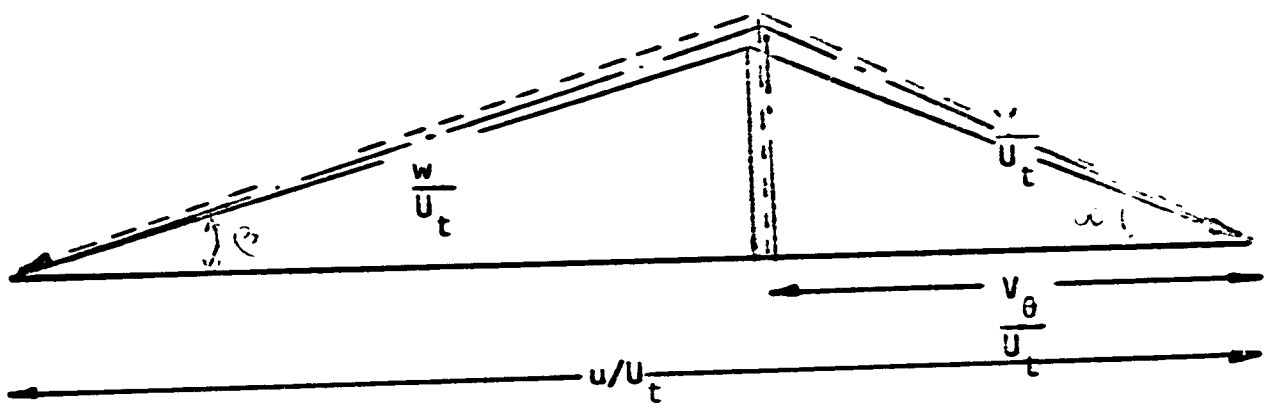

Scale 1" = 0.1

Fig. 16c Revised Comparison of velocity triangles derived from relative and absolute flow measurement $r/r_t = 0.55$, Station 4.

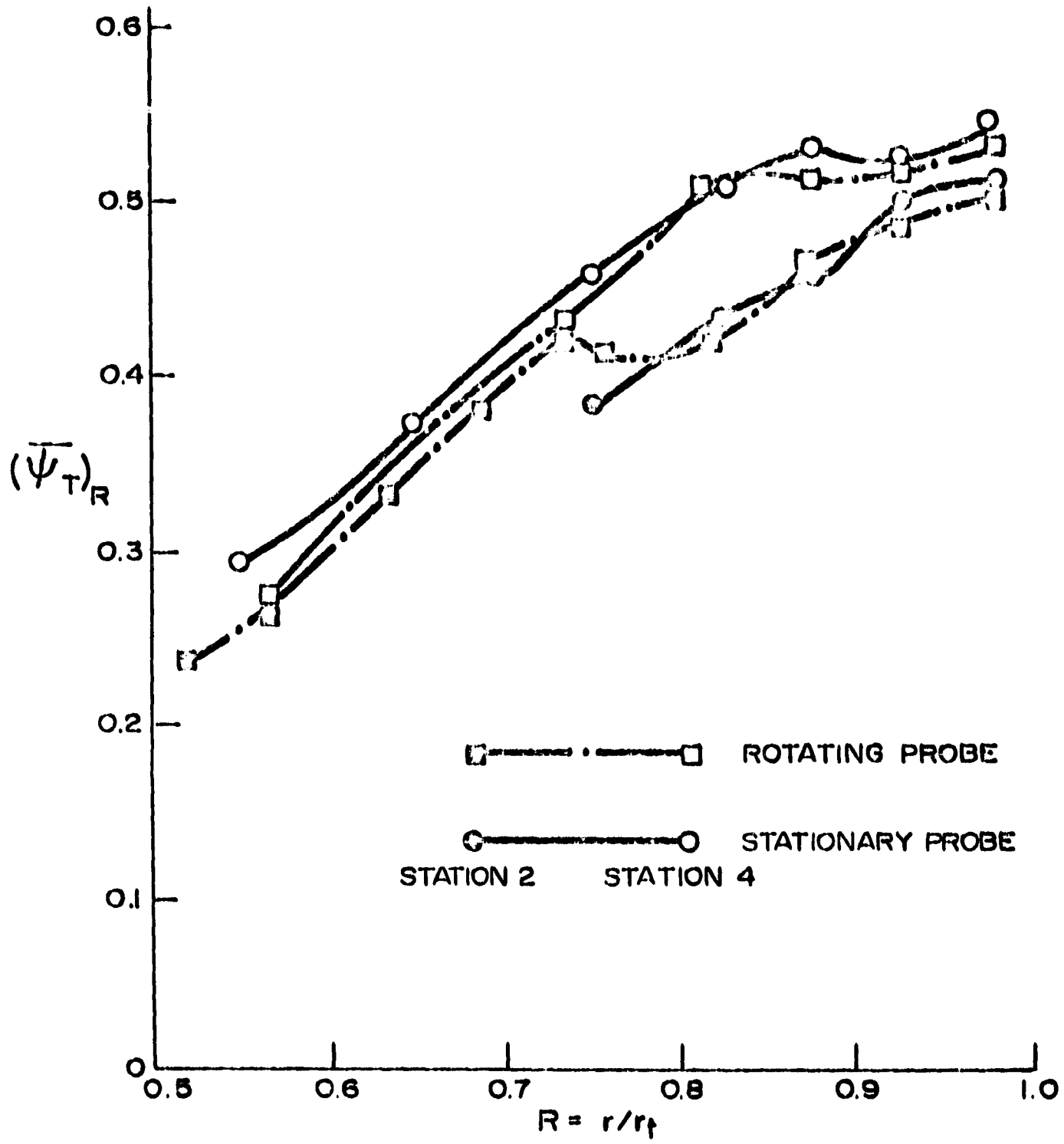

FIGURE 17. COMPARISON BETWEEN THE ROTATING AND THE STATIONARY PROBE MEASUREMENTS.